HEALTH AND MEDICINE

Strontium ions protect hearts against myocardial ischemia/reperfusion injury

Min Xing[1,2]*, Yun Jiang[3,4]*, Wei Bi[3,4], Long Gao[1,2], Yan-Ling Zhou[1,2], Sen-Le Rao[3,4], Ling-Ling Ma[1,2], Zhao-Wenbin Zhang[1,2], Huang-Tian Yang[3,4,5]†, Jiang Chang[1,2,5]†

Timely restoration of blood supply following myocardial infarction is critical to save the infarcted myocardium, while reperfusion would cause additional damage. Strontium ions have been shown to promote angiogenesis, but it is unknown whether they can save the damaged myocardium. We report that myocardial ischemia/reperfusion (I/R)–induced functional deterioration and scar formation were notably attenuated by injection of strontium ion–containing composite hydrogels into murine infarcted myocardium at 20 minutes of reperfusion following 60 minutes of ischemia. These beneficial effects were accompanied by reduced cardiomyocyte apoptosis and increased angiogenesis. The effects of strontium ions were further confirmed by the enhanced viability of cardiomyocytes and stimulated angiogenesis in vitro. These findings are the first to reveal the cardioprotective effects of strontium ions against I/R injury, which may provide a new therapeutic approach to ischemic heart disease at a lower cost, with higher stability, and with potentially greater safety.

INTRODUCTION

Myocardial infarction (MI) remains the major cause of morbidity and mortality worldwide (*1*). Early reperfusion during MI is critical for saving the myocardium, but it can cause new injury and limit the beneficial effects of reperfusion therapy (*2*). Therefore, various approaches for the protection of the heart from ischemia/reperfusion (I/R) injury have been extensively studied. Ischemic pre- and postconditioning (PoC) are well-explored strategies for the cardioprotection against reperfusion injury (*2*, *3*). However, they have limited values in the clinic application as requirement of predictability of ischemic situation and invasive interference (*4*, *5*). Instead, pharmacological interference at the beginning of reperfusion is more clinically feasible than mechanical PoC (*6*). However, there are limited agents clinically available for the patient with ischemic heart disease (*4*, *7*). In addition, cell therapy has been shown to promote the healing of the infarct hearts via improving neovascularization, cardiomyocyte survival, and/or remuscularizing the ischemic hearts (*8*–*10*). However, they are still facing challenges for clinical applications (*11*). Therefore, it is necessary to continuously explore and develop optimal approaches with therapeutic and practical characteristics for the treatment of MI (*12*), especially the simple and effective approaches aimed at protecting the heart against I/R injury, which would be of therapeutic significance.

Bioactive ions released from the bioceramics are of interest in the fields of regenerative medicine and tissue engineering owing to the possibility of exploiting their unique advantages for therapeutic applications: low cost, increased stability, and potentially lesser risk than techniques of recombinant proteins or genetic engineering (*13*). Cumulated studies have shown that bioactive ions could induce specific cellular response, stimulate proliferation and directional differentiation of diverse cells, and affect the cell-cell interactions, thereby promoting tissue and organ formation or regeneration (*14*). Currently, the ion treatment methods have been widely used in the multiple damaged tissue repair, such as bone, cartilage, teeth, adipose, and skin (*15*). In addition, we recently found that the transplantation of a silicate ceramic/polymer composite cardiac patch seeded with activated cardiomyocytes is effective to promote the repair of infarcted myocardial by promoting angiogenesis (*16*). These beneficial effects are associated with the stimulated angiogenesis and enhanced cardiomyocyte viability by the Si ions released from silicate bioceramics (*17*). These findings suggest that inorganic biomaterials with angiogenic bioactivity may be used for the soft tissue repair. However, it is unclear whether the bioactive ions can promote the infarct heart recovery from I/R injury.

Sr is an essential trace element in the human body, and Sr ion–containing biomaterials are traditionally considered as a product for bone repair. Sr-doped $CaSiO_3$ bioceramics have been found to promote angiogenesis of endothelial cells, and what is more, we recently found that Sr ions are more effective than Si ions in promoting blood vessel formation during bone regeneration (*18*). The high bioactivity in promoting angiogenesis implies that Sr ions may have angiogenic activity in heart tissue environment and that Sr-containing biomaterials may also be valuable for repairing infarcted hearts.

On the basis of these considerations, we innovatively confirmed the effects of Sr ions in the stimulating of angiogenesis and the maintaining of cardiomyocyte viability and then designed Sr ion–containing composite hydrogels with the Sr ion–releasing property for the treatment of myocardial I/R injury in mice. The effects of Sr ions on cardiac function improvement, blood vessel formation, and inhibition of cardiomyocyte apoptosis in vivo were investigated, and the mechanisms were explored by studying the cell-cell interaction in the presence of Sr ions. The previously unrecognized effects of Sr ions in promoting healing of infarct hearts via promoting angiogenesis and protecting cardiomyocytes are explicitly revealed in the present study. Our findings might provide a new strategy for the treatment of ischemic heart disease.

[1]State Key Laboratory of High Performance Ceramics and Superfine Microstructure, Shanghai Institute of Ceramics, Chinese Academy of Sciences (CAS), Shanghai 200050, P. R. China. [2]Center of Materials Science and Optoelectronics Engineering, University of CAS, Beijing 100049, P. R. China. [3]CAS Key Laboratory of Tissue Microenvironment and Tumor, Laboratory of Molecular Cardiology, Shanghai Institute of Nutrition and Health, CAS, Shanghai 200030, P. R. China. [4]University of CAS, 19 Yuquan Road, Beijing 100049, P. R. China. [5]Institute for Stem Cell and Regeneration, CAS, Beijing 100101, China.
*These authors contributed equally to this work.
†Corresponding author. Email: jchang@mail.sic.ac.cn (J.C.); htyang@sibs.ac.cn (H.-T.Y.)

RESULTS

The beneficial effects of Sr ions on cardiomyocytes and cardiovascular cells

The rescue of injured cardiomyocytes and angiogenesis is critical to repair infarcted myocardium. To determine the role of Sr ions in the maintenance of the viability of cardiomyocytes, we treated the cultivated neonatal rat cardiac myocytes (NRCMs) with Sr ions at various concentrations for 10 days (table S1). The analysis of quantitative real-time polymerase chain reaction (qRT-PCR) showed that the expression levels of cardiac-specific genes including *myosin heavy chain 6* (*Myh6*), *Myh7*, *calcium voltage-gated channel subunit α 1 A*, *gap junction protein α 1*, and *troponin T2* were significantly higher in the Sr ion–treated NRCMs at the range of 10 to 42 μg/ml (1/16 to 1/4 dilution of the extracts as shown in table S1) than those in the control ones (fig. S1). Moreover, we tested whether Sr ions can protect the cardiomyocytes from oxygen glucose deprivation (OGD) injury. Glucose/oxygen-deprived culture condition for 4 hours followed with 36 hours of normal culture condition induced the suppression of cell viability in the NRCMs, while this was improved by 44% (1/4 Sr), 73.26% (1/8 Sr), and 40.61% (1/16 Sr) in the Sr ion–treated NRCMs, respectively (Fig. 1A). Consistently, the OGD-induced terminal deoxynucleotidyl transferase-mediated deoxyuridine triphosphate nick end labeling–positive ($TUNEL^+$) cells were significantly reduced by Sr ions at the optimal concentration of 21 μg/ml (Fig. 1B).

In addition to the protection of cardiomyocytes, blood vessel formation is also vital to facilitate the repair of infarct myocardium (*19*). Considering that endothelial cells, fibroblasts, and smooth muscle cells are the main cells that form blood vessels and play different roles in angiogenesis, we examined the effects of Sr ions on these three types of cells under normal conditions. The Cell Counting Kit-8 (CCK8) analysis and immunofluorescent staining of proliferation maker Ki67 showed that all of these cells exerted higher cell viability and enhanced percentages of $Ki67^+$ cells after Sr ion treatment (Fig. 1, C to H). Moreover, wound healing assays, qRT-PCR, and Western blot analysis showed that the migration of human umbilical vein endothelial cells (HUVECs) and human dermal fibroblasts (HDFs) was enhanced (fig. S2) and the expression levels of angiogenesis-related genes (*19*) [*vascular endothelial growth factor* (*VEGF*), *kinase insert domain receptor* (*KDR*), *basic fibroblast growth factor* (*bFGF*), *bFGF receptor* (*bFGFR*), and *endothelial nitric oxide synthase* (*eNOS*)] were increased (fig. S3) after cultivating with the Sr ions under normal conditions. Moreover, Sr ions significantly increased the expression of proliferation-related genes—such as [*cellular FOS proto-oncogene* (*C-FOS*), *cellular MYC proto-oncogene* (*C-MYC*), *cellular SIS proto-oncogene* (*C-SIS*), and *early growth response 1* (*EGR-1*)]—and promoted the migration of human umbilical vein smooth muscle cells (HUVSMCs) under normal conditions (fig. S4). All of these active concentrations were in the range of 10 to 42 μg/ml (1/16 to 1/4 dilution of the extracts as shown in table S1). These results suggest that Sr ions have robust ability in the stimulating of angiogenesis-associated cells by enhanced cell proliferation and migration, which implies the therapeutic potential of Sr ions in promoting repair of ischemic hearts.

Sr ions stimulate the angiogenic effects of cardiac cells via strengthening their paracrine capacity in vitro

As the Sr ions benefit various types of cells, it is possible that Sr ions could harmonically affect various cardiac cells. Since it is important and essential to the interaction between cells in the cardiac tissue, where blood vessel–forming cells and cardiomyocytes coexist (*17*), we thus investigated the cell-cell interaction in the presence of Sr ions in relation to the angiogenesis using both direct and indirect coculture models (Fig. 2A).

First, we studied the effects of Sr ions on the angiogenic function in the direct or indirect cocultured HUVECs and NRCMs (Fig. 2A). One day after coculture of HUVECs and NRCMs with equal cell number, we treated the mixed cells with or without Sr ions and found that the HUVECs presented more tube networks in the Sr ion–treated group through von Willebrand factor (vWF) staining after 3 days of cultivation (Fig. 2B). To investigate whether there are synergistic effects, we collected the HUVECs and NRCMs from monoculture and separated these cells from directly contacting cocultured system using magnetic bead separation with or without Sr ion treatment. The qRT-PCR analysis showed that, under the normal culture condition (control), the coculture increased the expression of the angiogenesis-related genes in the HUVECs, such as *VEGF*, *KDR*, *vascular endothelial–cadherin* (*VE-cad*), *eNOS*, *bFGF*, and *bFGFR*, compared with those in the monocultured HUVECs (Fig. 2C). Similarly, the collected NRCMs from the cocultured HUVECs with NRCMs also expressed higher levels of angiogenic genes, such as *VEGF*, *eNOS*, *bFGF*, and *bFGFR*, than those in the monocultured NRCMs (Fig. 2C). Sr ions not only enhanced the expression of these genes in the HUVECs and NRCMs cultured alone but also further improved the expression of these angiogenesis-related genes in the HUVECs and NRCMs collected from the coculture system (Fig. 2C).

Then, we analyzed the gene expression in the indirect cocultured HUVECs and NRCMs with or without Sr ion treatment. The qRT-PCR analysis showed that the Sr ions stimulated both HUVECs and NRCMs to express higher angiogenesis-related genes, such as *VEGF*, *KDR*, *VE-cad*, *eNOS*, *bFGF*, and *bFGFR* (*KDR* and *VE-cad* were only increased in HUVECs) with a similar activation pattern as that for the direct HUVEC-NRCM coculture (Fig. 2D). Moreover, similar to the results of enhanced expression of angiogenic genes in HUVECs after treated with the conditioned medium from NRCMs without Sr ions, the expression of angiogenic genes in the NRCMs also increased after cultured with the conditioned medium from HUVECs without Sr ions (Fig. 2D). After Sr ion treatment, these cell conditioned media showed much higher intensive induction of the angiogenic genes mentioned above (Fig. 2D). These findings suggest that the paracrine effects of NRCMs activated by Sr ions also contribute to the enhanced angiogenesis in addition to the direct activation of HUVECs by Sr ions.

In addition to the interaction of cardiomyocytes and endothelial cells, the interwork of endothelial cells and fibroblasts is also important during blood vessel formation and particularly crucial in the early stage of angiogenesis (*20*). Therefore, we analyzed the effects of Sr ions on the cocultured HUVECs and HDFs. The vWF staining analysis revealed that the direct coculture of HUVECs with HDFs in the Sr ion–containing medium formed better tubule networks than that without Sr ion treatment (fig. S5A). The analysis of qRT-PCR showed that the cocultured cells (HUVECs and HDFs) expressed higher levels of angiogenesis-related genes as respectively compared with the monocultured ones (fig. S5B). Moreover, the monocultured and cocultured HUVECs both expressed higher levels of *bFGF*, *bFGFR*, *VEGF*, *KDR*, *eNOS*, and *VE-cad* in the presence of Sr ions as compared with that cultured without Sr ions (fig. S5B). Simultaneously, Sr ions also stimulated higher expression of angiogenic genes including *bFGF*, *bFGFR*, *VEGF*, and *eNOS* in the monocultured

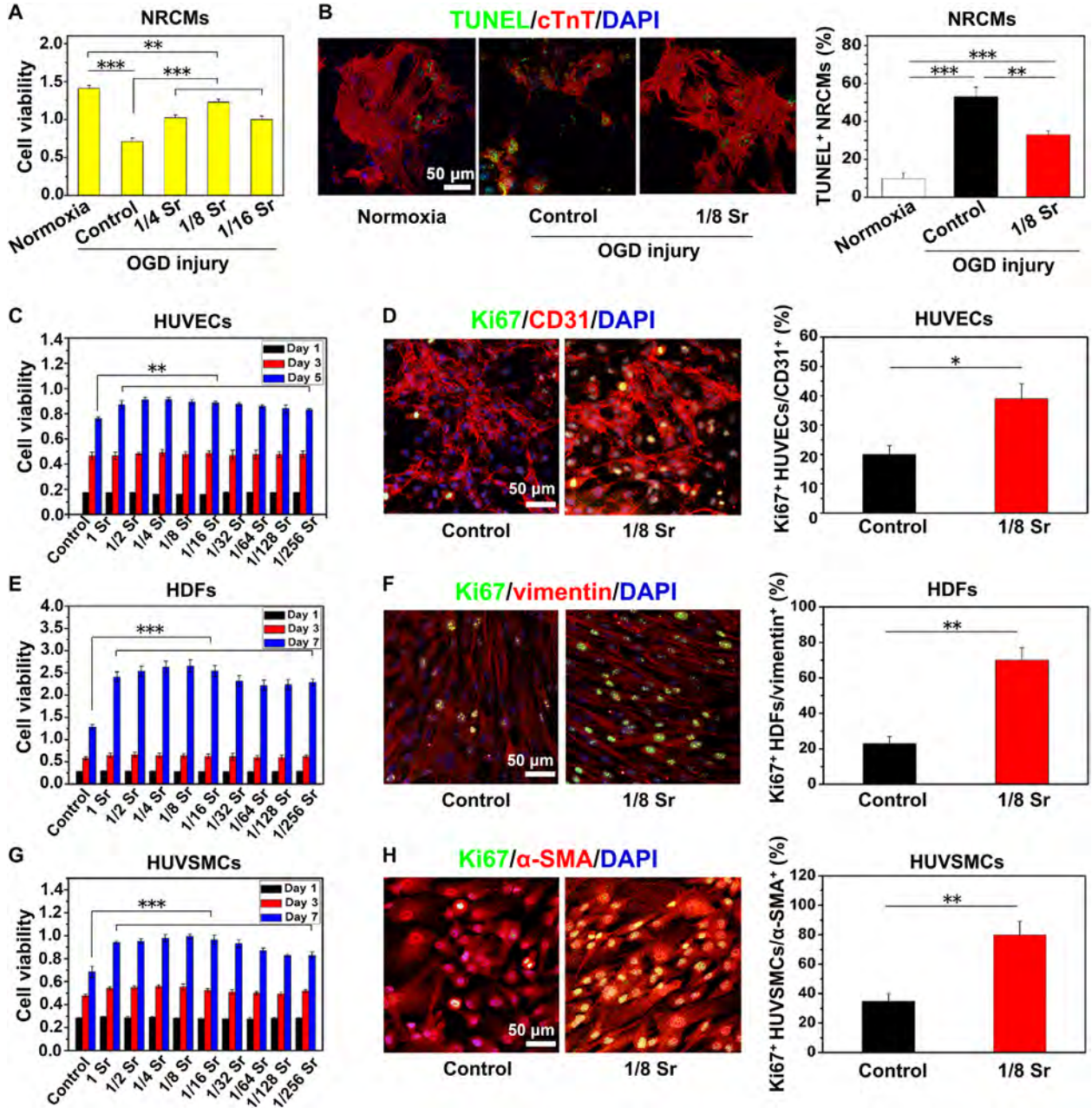

Fig. 1. Sr ions reduce NRCM apoptosis after OGD injury and promote blood vessel–related cell proliferation. (**A**) The viability of NRCMs measured by Cell Counting Kit-8 (CCK8) in the medium supplemented with different concentrations of Sr ion after OGD injury. (**B**) TUNEL staining (green), cTnT staining (red), and DAPI (4′,6-diamidino-2-phenylindole) staining (blue) in NRCMs after OGD injury and quantitative analysis of TUNEL$^+$ NRCMs (10 pictures for each group). The corresponding concentrations of Sr ion with the 1/4 to 1/16 dilution ratio for NRCM culture are shown in table S1. (**C** to **H**) The cell viability and proliferation of human umbilical vein endothelial cells (HUVECs) (C and D), human dermal fibroblasts (HDFs) (E and F), and human umbilical vein smooth muscle cells (HUVSMCs) (G and H) after culturing in the medium supplemented with Sr ions at different concentrations. They were respectively revealed by CCK8 and the immunofluorescence of Ki67, followed by quantitative analysis of Ki67$^+$ after Sr ion treatment for 5 days (HUVECs) or 7 days (HDFs and HUVSMCs). The corresponding concentrations of Sr ion with the dilution ratio of 1 to 1/256 for HUVEC, HDF, and HUVSMC culture are respectively shown in table S1. Experiments were conducted in triplicate. All data are presented as means ± SEM. An unpaired *t* test was used to compare between any two groups. One-way analysis of variance (ANOVA) was used to compare between three or more groups. **P* < 0.05, ***P* < 0.01, and ****P* < 0.001.

or cocultured HDFs (fig. S5B). The Sr ions even activated HDFs expressing a higher level of *VEGF* than those in the HUVECs both under the monoculture and coculture conditions, but not the downstream angiogenic molecules, such as *KDR* and *eNOS* (fig. S5B). Furthermore, in an indirect contact coculture model of HUVECs and HDFs, a similar activation pattern of the gene expression was observed (fig. S5C). The conditioned medium collected from the HDFs (without Sr ion treatment) stimulated HUVECs to express higher levels of *bFGF*, *bFGFR*, *VEGF*, *KDR*, *eNOS*, and *VE-cad* (fig. S5C). Meanwhile, HDFs cultured with the conditioned medium

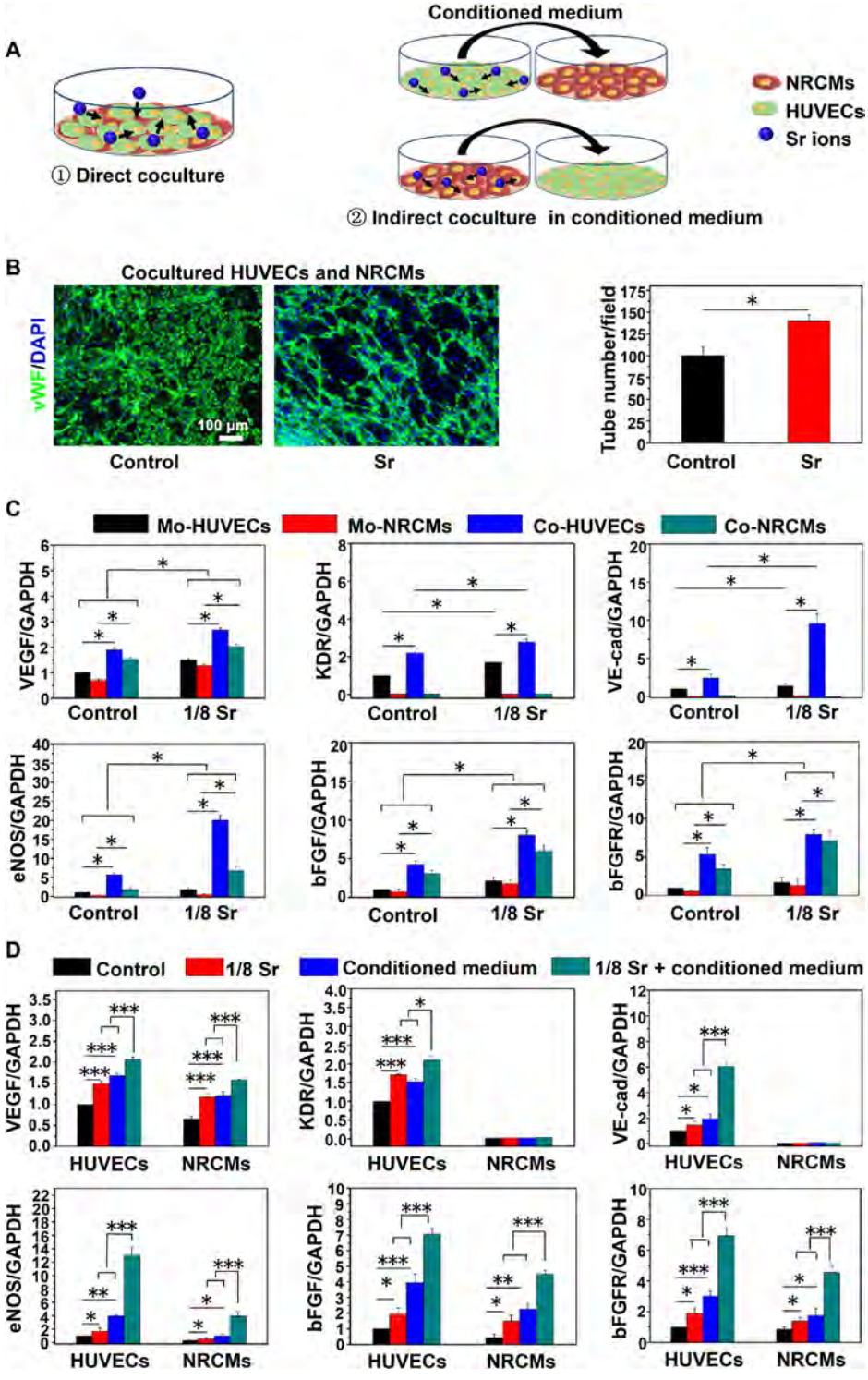

Fig. 2. Sr ions stimulate paracrine-mediated angiogenic effects of HUVECs and NRCMs after 3 days of coculture. (**A**) Schematic of direct and indirect coculture of HUVECs and NRCMs. (**B**) Images and quantitative analysis of von Willebrand factor (vWF) staining for the tube formation ability of cocultured HUVECs with control medium and Sr ion–containing medium (10 pictures for each group). An unpaired *t* test was used for statistical analyses. **P* < 0.05. (**C**) qRT-PCR analysis of the expression levels of angiogenesis-related genes [*VEGF*, *KDR*, *vascular endothelial–cadherin* (*VE-cad*), *eNOS*, *bFGF*, and *bFGFR*] in HUVECs and NRCMs that were acquired from monocultured cells or cocultured cells in each treatment group. Experiments were conducted in triplicate. An unpaired *t* test was used for statistical analyses. All data are presented as means ± SEM. **P* < 0.05 was considered statistically significant. Mo, monocultured; Co, cocultured. (**D**) qRT-PCR analysis of the angiogenic gene (*VEGF*, *KDR*, *VE-cad, eNOS*, *bFGF*, and *bFGFR*) expression in HUVECs treated with normal medium and conditioned medium from NRCMs, which were treated with Sr ions or not, as well as in NRCMs treated with normal medium and conditioned medium from HUVECs, which were treated with Sr ions or not. Experiments were conducted in triplicate. One-way ANOVA was used for statistical analyses. All data are presented as means ± SEM. **P* < 0.05, ***P* < 0.01, and ****P* < 0.001.

collected from the HUVECs (without Sr ion treatment) also expressed higher levels of *bFGF*, *bFGFR*, *VEGF*, and *eNOS* (fig. S5C). Consistently, after Sr ion treatment, conditioned medium showed much higher intensive induction of the angiogenic genes mentioned above (fig. S5C). Thus, similar to that in the coculture of HUVECs and NRCMs, paracrine effects in the coculture of HUVECs and HDFs activated by Sr ions significantly contribute to the enhanced angiogenesis.

The proliferation of HUVSMCs is further enhanced by the interaction between HUVECs and HUVSMCs with the stimulation of Sr ions in vitro

In addition to angiogenesis, which is the primary step of the infarcted myocardial tissue repair and cardiac function recovery via providing the needed nutrients for tissue repair (*19*), arteriogenesis also plays an essential role for reestablishing blood network after ischemic injury (*21*). Smooth muscle cells are located near endothelial cells, and their proliferation plays an irreplaceable role in the development and maturation of collateral coronary artery (*22*, *23*). We have found in the first part of this study that Sr ions stimulated HUVSMC proliferation. Then, we observed that, in the direct cocultures of HUVECs and HUVSMCs, the expression level of *platelet-derived growth factor subunit B* (*PDGFB*) was similar in the separated HUVECs from monocultured or cocultured cells, but it was increased after treated with Sr ions in the above cultural methods (Fig. 3A). In the cocultured HUVSMCs with HUVECs without Sr ions, the expression of *PDGF receptor* β (*PDGFRB*), a receptor of PDGFB, and proliferation-related genes (*C-FOS*, *C-MYC*, *C-SIS*, and *EGR-1*) was significantly higher than those in the monoculture HUVSMCs. Meanwhile, Sr ion treatment of cocultured cells further promoted the expression of these genes as compared with those without Sr ion treatment (Fig. 3A). Simultaneously, in the indirect contact coculture system of HUVECs and HUVSMCs, a similar activation pattern of gene expression was observed (Fig. 3B). The conditioned medium from HUVSMCs failed to increase the expression of *PDGFB* in

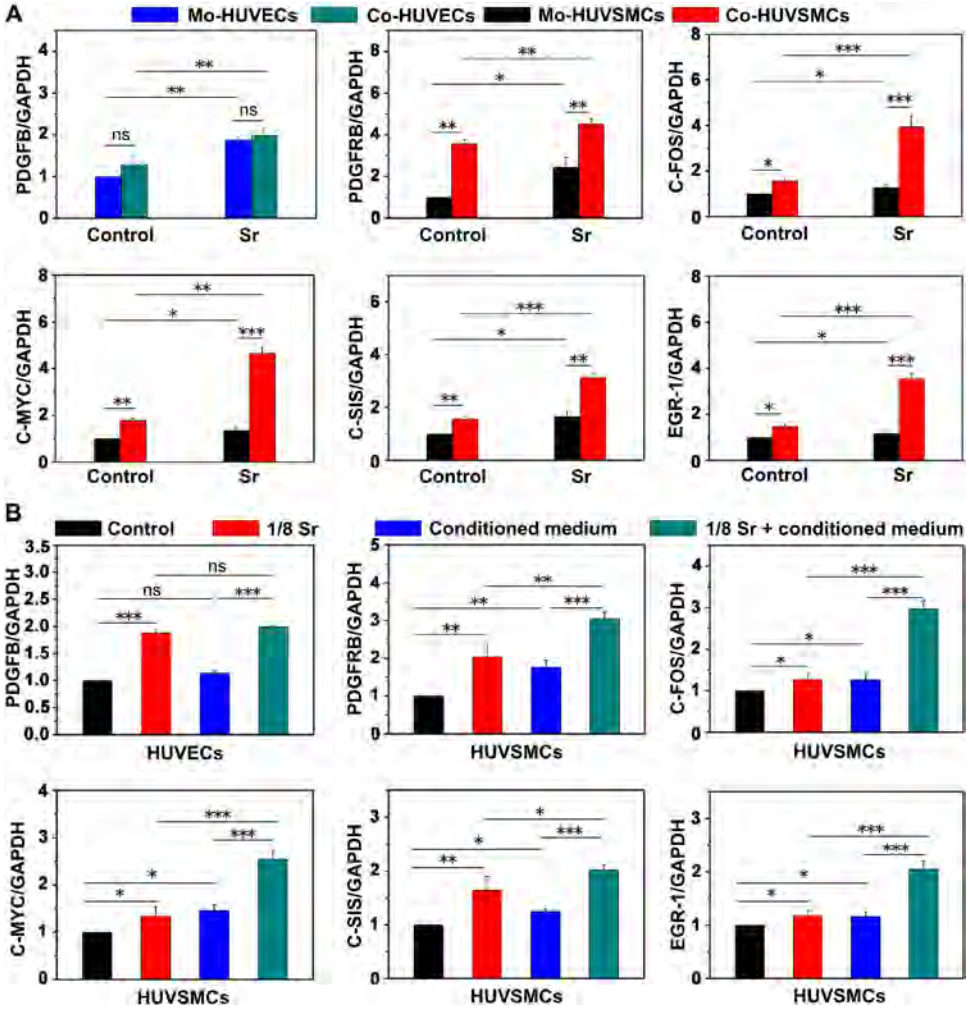

Fig. 3. Sr ions stimulate paracrine-mediated proliferation effects of HUVSMCs after 3 days of coculture with HUVECs. (**A**) qRT-PCR analysis of the expression levels of *PDGFB* in monocultured HUVECs and cocultured HUVECs and gene expression of *PDGFRB*, *C-FOS*, *C-MYC*, *C-SIS*, and *EGR-1* in monocultured HUVSMCs and cocultured HUVSMCs in each treatment group. An unpaired *t* test was used for statistical analyses. (**B**) qRT-PCR analysis of the expression levels of *PDGFB* in HUVECs treated with conditioned medium from HUVSMCs with or without Sr ions and gene expression of *PDGFRB*, *C-FOS*, *C-MYC*, *C-SIS*, and *EGR-1* in HUVSMCs treated with conditioned medium from HUVECs with or without Sr ions. Experiments were conducted in triplicate; one-way ANOVA was used for statistical analyses. All data are presented as means ± SEM. **P* < 0.05, ***P* < 0.01, and ****P* < 0.001. ns, no statistical significance.

HUVECs, while the conditioned medium from HUVECs significantly enhanced the proliferation-related gene expression in HUVSMCs, which was further improved by the Sr ion treatment. These results suggest that the Sr ions have the ability to induce paracrine effects of the HUVECs involved in the interconnecting and proliferation of HUVSMCs.

Design and preparation of $SrCO_3$/albumin composite hydrogels with injectability

To test the effects of Sr ions on the infarcted heart repair and apply Sr ions in vivo, we then designed a composite hydrogel with an ability to sustain the release of Sr ions. Although the optimal concentration for the proliferation of HUVECs (42 μg/ml) appeared to be slightly higher than those for the proliferation of the HDFs and HUVSMCs as well as the protection of NRCMs (21 μg/ml), the lower concentration of Sr ion (21 μg/ml) was able to activate all three types of blood vessel–forming cells and cardiomyocytes (Fig. 1). To obtain effective concentration of Sr ion for the infarcted myocardium repair in vivo, we selected 21 μg/ml (1/8 dilution of the extracts) as the concentration of Sr ion for the design of the Sr-releasing hydrogel.

As shown in the design schematic of the $SrCO_3$/albumin composite hydrogels (Fig. 4A), $SrCO_3$/human serum albumin (HSA) composite hydrogels were prepared with different amount of $SrCO_3$ [D50 (median particle diameter) = 4.192 μm as shown in Fig. 4D] to obtain hydrogels with suitable physical properties and release Sr ions in the optimal bioactive concentration. The hydrogels were formed on the basis of the cross-linking reaction between the free amino groups of the HSA and two-arm succinimidyl active ester groups of poly(ethylene glycol) disuccinimidyl succinate [PEG-$(SS)_2$], and the gelation time mainly depended on the nucleophilicity of the amino groups, which could be regulated by the pH of the polymerization reaction (Fig. 4C). Since the alkaline environment generated by $SrCO_3$ hydrolysis also regulated the gelling time of the $SrCO_3$/HSA hydrogels cross-linked with PEG-$(SS)_2$, we observed that the color and gelling time of the hydrogels were dependent on the amount of $SrCO_3$ added in the HSA (Fig. 4, B and E). In general, the gelling time was in the range of 3 to 10 min, and this may meet the requirement for readiness period before using the injectable hydrogels in different situations. Our results showed that 1% $SrCO_3$ and 2% $SrCO_3$/HSA composite hydrogels were tolerable for gel formation and injection. Moreover, the active esters in the hydrogels had the ability to bond with amino groups on the surface of tissue, which may be conducive to its adhesion in myocardial tissue (*24*).

To verify the optimal releasing concentration of Sr ion, we evaluated the concentrations of Sr ions released from hydrogels with different $SrCO_3$ amounts. The analysis showed that, during a 9-day cultivation time, the concentrations of Sr ions released from each group did not change significantly, indicating a sustained release of Sr ions from the HSA hydrogels (Fig. 4F). Among the three groups, the Sr ion–releasing concentration of HSA hydrogels with 1% $SrCO_3$ (22.61 ± 1.80 μg/ml to 20.61 ± 1.00 μg/ml) was more consistent with the optimal concentrations of Sr ion obtained from in vitro experiment results (Fig. 1 and figs. S1 to S4). Thus, we used 1% $SrCO_3$/HSA hydrogels for the further study.

To study the effect of $SrCO_3$ powder composition on the physical properties of hydrogels, we investigated the elastic moduli (G') and viscous moduli (G'') of hydrogels as a function of the strain (Fig. 4G) and frequency (Fig. 4H) by rheological characterization. As shown in Fig. 4G, the intersection positions of the G' and G'' curves corresponding to the HSA hydrogels and 1% $SrCO_3$ composite HSA hydrogels were similar, indicating that the strain value of these two kinds of hydrogels was nondistinctive when they were damaged and the recombination of $SrCO_3$ powders did not change the toughness of HSA hydrogels. As shown in Fig. 4H, G' and G'' curves of the hydrogels (HSA and HSA + 1% Sr) showed frequency independence. In addition, the G' was greater than G'' for these two kinds of hydrogels over the entire range of frequency, which indicated the good stability of three-dimensional network in the gel system.

The in vitro degradation experiment may be used to predict the in vivo degradation process of hydrogels and particle compound in hydrogels; thus, the in vitro degradation behavior of the HSA hydrogels, 1% $SrCO_3$/HSA composite hydrogels, and the inside $SrCO_3$ powders were evaluated by soaking the samples in tris-HCl buffer solution (pH 7.4). As shown in Fig. 4I, the weight loss of the HSA hydrogels, 1% $SrCO_3$/HSA composite hydrogels, and the $SrCO_3$ powders inside hydrogels respectively reached 50.68 ± 4.680%, 51.982 ± 3.631%, and 57.417 ± 3.083% after 14 days. These results indicated that the combination of $SrCO_3$ powders did not change the degradation rate of hydrogels. As compared with $SrCO_3$ powders, the degradation of the composite hydrogels was slightly slower, but there was no significant difference.

Therapeutic effects of the $SrCO_3$/HSA composite hydrogels after intramyocardially injected in the murine I/R hearts

The $SrCO_3$/HSA composite hydrogels improve cardiac function of I/R hearts

Then, we tested the hypothesis that the released Sr ions from transplanted $SrCO_3$/HSA composite hydrogels could serve as myocardial protective elements for the ischemic heart repair. We compared the functional outcomes of mice among different groups: I/R + control, I/R + HSA hydrogels (I/R + HSA), and I/R + 1% $SrCO_3$/HSA composite hydrogels (I/R + HSA + 1% Sr) at days 1 and 28 after I/R as indicated in Fig. 5A. The 9.1% mortality was observed in the I/R control group (1 death of 11), but no one died in the I/R mice treated with HSA hydrogels or 1% $SrCO_3$/HSA composite hydrogels during the 28-day follow-up period (Fig. 5B). The body weights of the mice in the three groups showed a transient decline tendency at day 1 after I/R but no significant difference among different groups (Fig. 5C). However, the left ventricular (LV) ejection fraction (LVEF) and LV fraction shortening (LVFS) were significantly improved by the $SrCO_3$/HSA composite hydrogel treatment as compared with the I/R control and HSA hydrogel groups at day 28 after I/R (Fig. 5, D and E). These data indicate the therapeutic benefit of Sr ions in improving heart function after I/R injury.

To verify the vital role of the sustained release of Sr ions from the composite hydrogels in the treatment, we further compared the injection of pure Sr ion solution with $SrCO_3$/HSA composite hydrogels. The results revealed that only the injection of $SrCO_3$/HSA composite hydrogels resulted in significant improvement of heart function at day 28 after I/R. The LVEF and LVFS of mice in the pure Sr ion solution–treated group did not show distinct improvement as compared with those in the I/R group, while these parameters significantly increased after the treatment with $SrCO_3$/HSA composite hydrogels (fig. S6A). Accordingly, the concentration of Sr ions in the mouse heart and serum dropped to normal levels at day 1 after injection in the Sr ion–alone group, while they were still higher than normal levels even at day 7 after injection in the $SrCO_3$/HSA composite hydrogel group (fig. S6B).

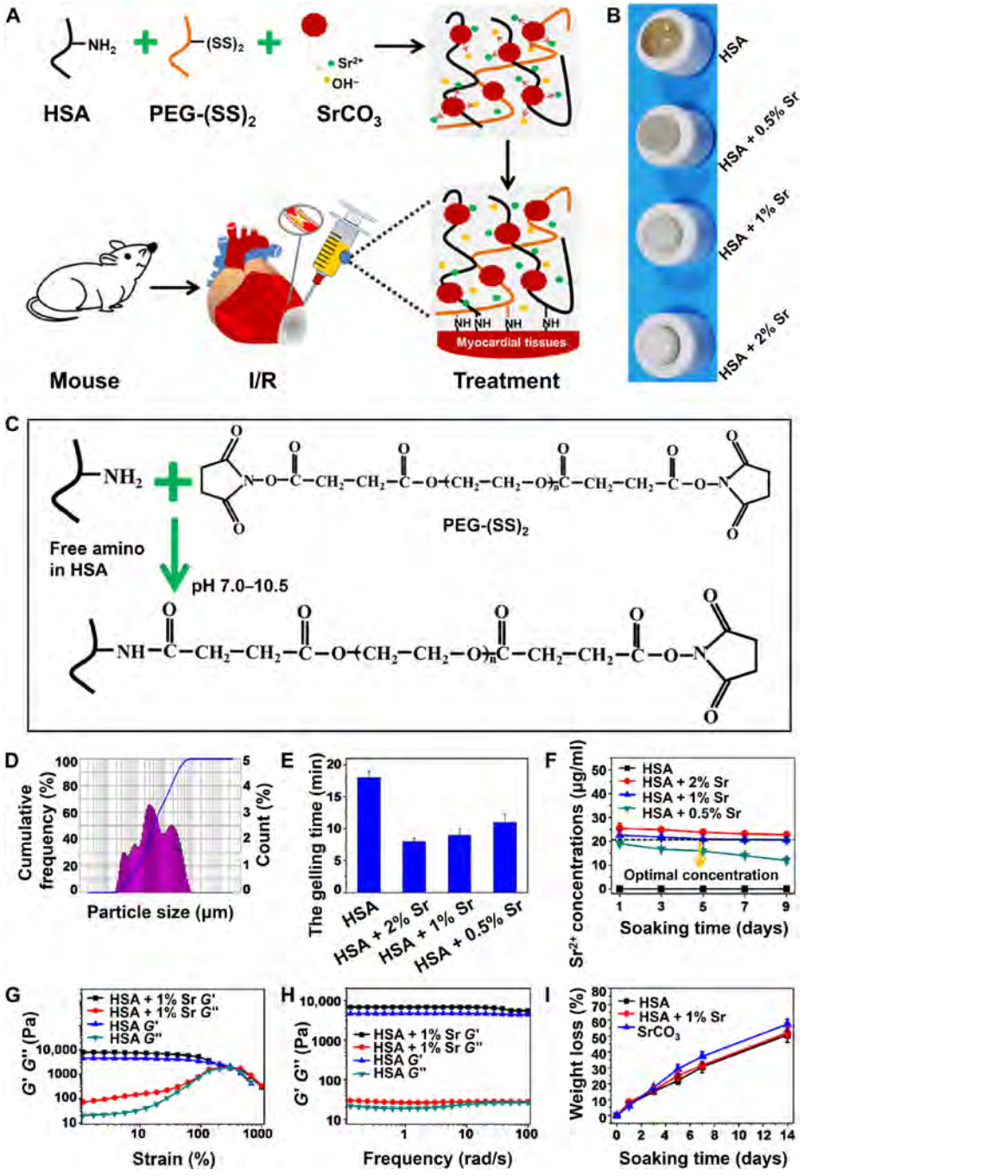

Fig. 4. Construct of injectable $SrCO_3$/HSA composite hydrogels (HSA). (**A**) Design schematic of $SrCO_3$/HSA composite hydrogels for injection into I/R mice. (**B**) The pictures of $SrCO_3$/HSA composite hydrogels with different $SrCO_3$ contents. (**C**) The gelation mechanism and chemical reactions between HSA and PEG-$(SS)_2$. (**D**) The particle size distribution of the $SrCO_3$ powder. (**E**) Gelling time of $SrCO_3$/HSA composite hydrogels. (**F**) Concentrations of Sr ions released from hydrogels. Experiments were conducted in triplicate. (**G**) Elastic moduli (*G*′) and viscous moduli (*G*″) as a function of the strain of HSA hydrogel and HSA + 1% Sr composite hydrogel. (**H**) *G*′ and *G*″ as a function of the frequency of HSA hydrogel and HSA + 1% Sr composite hydrogel. (**I**) The weight loss of the HSA hydrogel, HSA + 1% Sr composite hydrogel, and $SrCO_3$ powders inside the HSA + 1% Sr composite hydrogel after soaking in tris-HCl buffer solution (pH 7.4) at different time points. Experiments were conducted in triplicate. All data are presented as means ± SEM. (Photo credit: Min Xing, State Key Laboratory of High Performance Ceramics and Superfine Microstructure, Shanghai Institute of Ceramics, Chinese Academy of Sciences, Shanghai 200050, P. R. China.)

$SrCO_3$/HSA composite hydrogels increase angiogenesis, reduce cardiomyocyte apoptosis, and inhibit myocardial fibrosis

To explore the underlying mechanisms of improved heart function by $SrCO_3$/HSA, we implemented multiple histological analyses. All mice showed myocardial fibrosis formation at day 28 after I/R as analyzed by Masson's trichrome staining, while the myocardial fibrosis area in the 1% $SrCO_3$/HSA composite hydrogel–treated group was smaller than those in the I/R and HSA hydrogel groups (Fig. 6A).

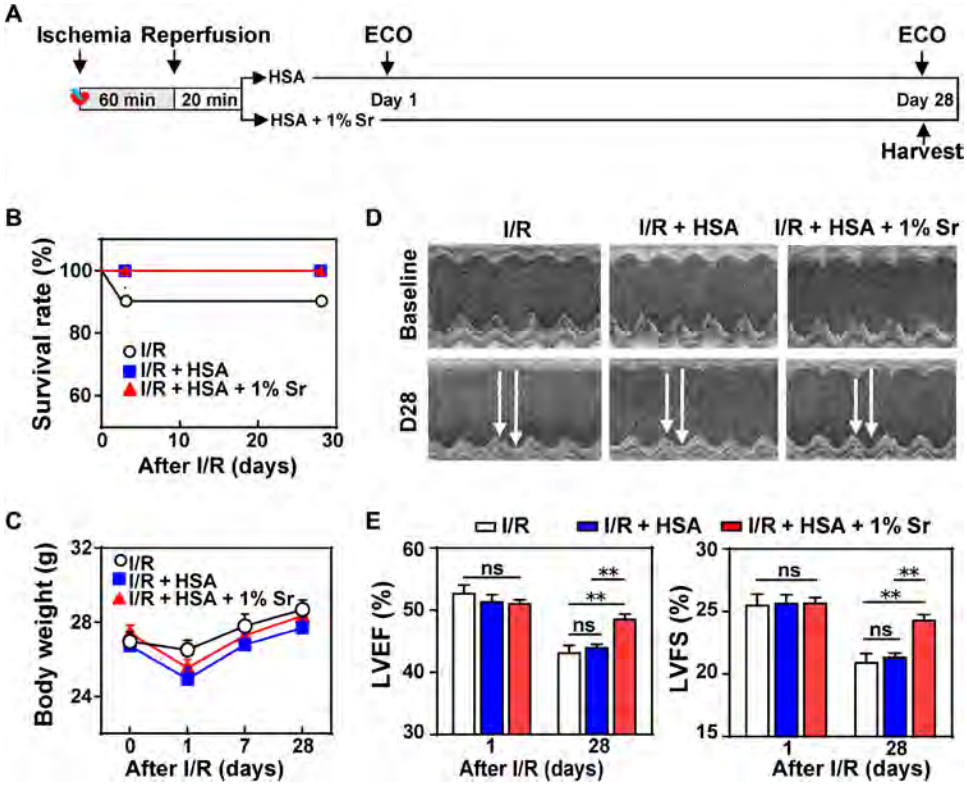

Fig. 5. $SrCO_3$/HSA hydrogels improve the recovery of mice cardiac function after I/R. (**A**) Schematic of I/R model establishment, hydrogel injection, and echocardiography (ECO) analysis. (**B**) Kaplan-Meier survival curves of mice during the 28 days after I/R. (**C**) Body weights of mice after I/R. (**D**) Representative echocardiograms obtained from the mid-papillary muscle region of the left ventricle of mice at day 28 (D28) after I/R. (**E**) Cardiac function measured by the percentage of LVEF and LVFS at days 1 and 28 after I/R. $n = 10$ each. All data are presented as means ± SEM. Comparisons between three groups were performed using two-way ANOVA. $^{**}P < 0.01$.

Considering that the reduction of myocardial fibrosis may be due to the improved angiogenesis and/or cardiomyocyte survival, we examined the number of α–smooth muscle actin–positive (α-SMA^+) blood vessels and $CD31^+$ cells in the border zone of infarcted hearts at day 28 after I/R. More α-SMA^+ blood vessels in tubular shape (Fig. 6B) and $CD31^+$ cells (Fig. 6C) were observed in the heart slices of the $SrCO_3$/HSA composite hydrogel group as compared with those in the I/R control and I/R + HSA hydrogel groups, which indicates an increased formation of arterioles and blood capillary (*25*, *26*). Consistently, the $SrCO_3$/HSA composite hydrogel significantly enhanced VEGF and eNOS levels in the infarct heart as determined by Western blot analysis at day 7 after I/R, while the HSA hydrogel and Sr ion solution did not improve the level of VEGF and eNOS (fig. S6C). Furthermore, the immunofluorescence staining analysis also showed that the $SrCO_3$/HSA composite hydrogel increased the VEGF level in the infarct heart at day 28 after I/R (Fig. 6D). Moreover, the number of $TUNEL^+$ cardiomyocytes detected in the border zone of day 3 infarcted hearts was significantly reduced after treated with $SrCO_3$/HSA composite hydrogels when compared with the other two groups (Fig. 6E). Accordantly, the $SrCO_3$/HSA composite hydrogels reduced the I/R-cleaved caspase-3 (Fig. 6, F and G) in the infarct myocardium and decreased the release of an injury marker lactate dehydrogenase (LDH) in the serum (Fig. 6H) of mice at day 3 after I/R. These data indicate that Sr ions improve the cardiac function through promoting blood vessel formation and inhibiting cardiomyocyte apoptosis in the infarct hearts.

Besides cardiomyocytes and endothelial cells, the cardiac fibroblasts are one of key cellular components in LV remodeling of post-MI hearts, which can be activated to generate anti-inflammatory and proangiogenic factors and secrete extracellular matrix components that may form the infarct scar (*27*). Since the proliferated and activated resident cardiac fibroblasts are considered as the main source of myofibroblasts in the infarct tissue and Sr ions also improved the proliferation of fibroblasts, we further investigated the effect of Sr ions on the activation of adult mice cardiac ventricle fibroblasts (AMVFs) and the viability of hypertrophic scar–derived fibroblasts (HSFs). After treating AMVFs and HSFs with Sr ions (21 μg/ml, 1/8 Sr), we analyzed the expression of α-SMA in AMVFs, which are most commonly used as the marker of myofibroblasts, and the cell viability of HSFs. As shown in fig. S7 (A and B), the expression of α-SMA was significantly enhanced after transforming growth factor–β (TGF-β) treatment, while Sr ions did not show activity to stimulate α-SMA expression after 1 day of cultivation with Sr ions. In addition, Sr ions did not affect the viability of HSFs (fig. S7C). These results suggest that the treatment of Sr ions may not result in scar formation by activating fibroblasts and improving the growth of myofibroblasts.

Metabolism and degradation of $SrCO_3$/HSA composite hydrogels in mice with myocardial I/R

To test whether Sr ions could be released from the transplanted hydrogels to the damaged hearts in a bioactive concentration range, we determined the concentrations of Sr ion in the hearts and serums

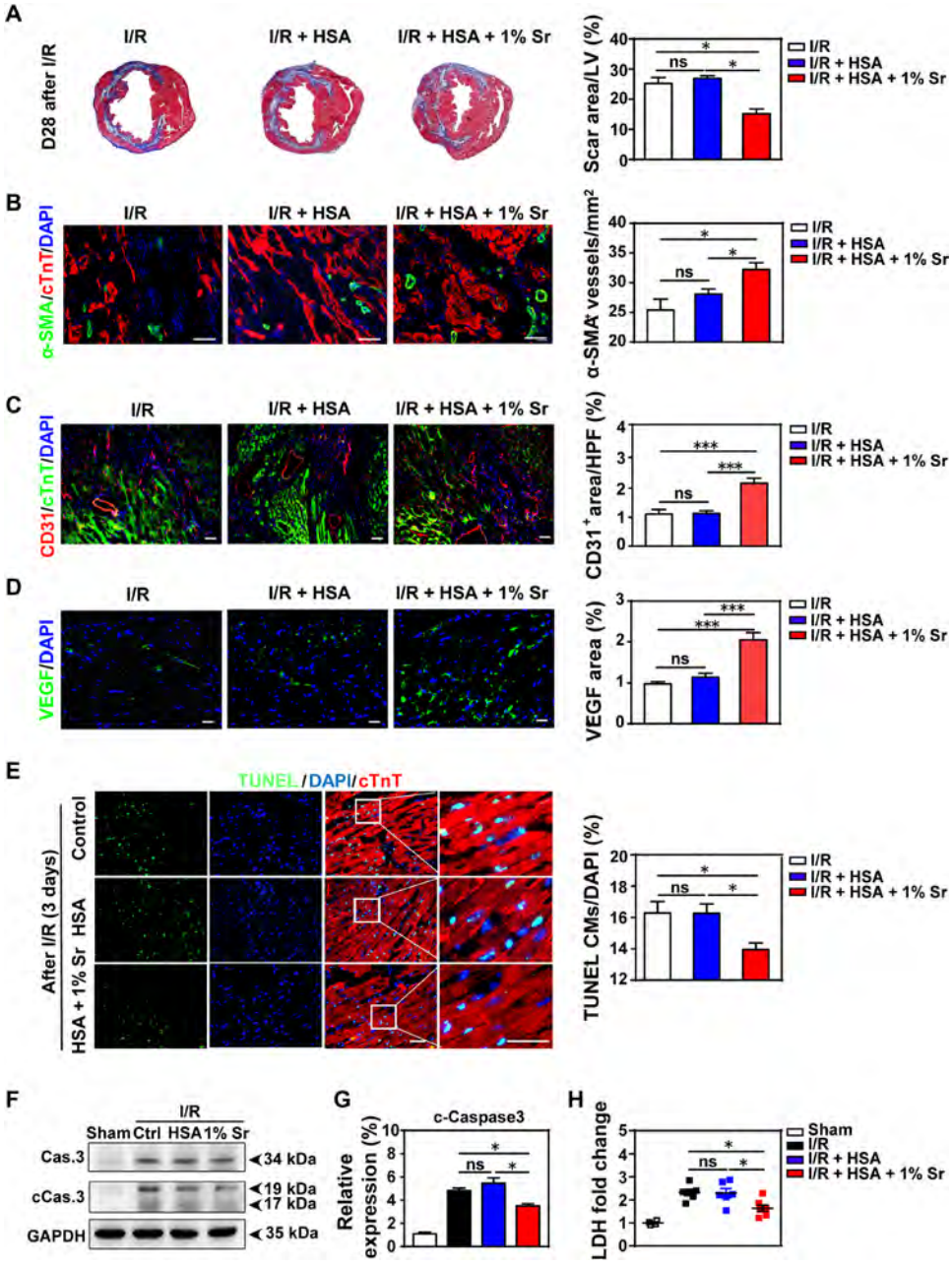

Fig. 6. $SrCO_3$/HSA hydrogels inhibit myocardial fibrosis, increase angiogenesis, and reduce cardiomyocyte apoptosis. (**A**) Representative cross-sectional images and quantitative data of scar area in LV on 5-μm slices stained with Masson's trichrome at day 28 after I/R. $n = 5$ hearts for each group. (**B** to **D**) Images and quantification of α-SMA$^+$ blood vessels (B), CD31$^+$ cells (C), and VEGF (D) in the border zone of infarcted hearts 28 days after I/R. Scale bars, 50 μm. $n = 4$ hearts for each group. HPF, high-power field. (**E**) Representative and quantification of staining for TUNEL$^+$ cardiomyocytes (CMs) in the border zone of infarcted hearts at day 3 after I/R. Scale bars, 50 μm. $n = 5$ to 6 hearts for each group. (**F** and **G**) Representative and averaged Western blot analysis for cleaved caspase-3 (cCas.3) and glyceraldehyde 3-phosphate dehydrogenase (GAPDH) in LV heart tissues at day 3 after I/R. $n = 4$ hearts each. (**H**) The concentrations of cardiac injury marker LDH of the mice serum at day 3 after I/R. $n = 4$ to 6 hearts each. Ctrl, I/R control; HSA, I/R + HSA; 1% Sr, I/R + HSA + 1% Sr. All values are expressed as means ± SEM; one-way ANOVA was used for statistical analyses. *$P < 0.05$ and ***$P < 0.001$.

after injection of $SrCO_3$/HSA composite hydrogels. The analysis of inductively coupled plasma atomic emission spectrometry showed that the initial concentration of Sr ions in the hearts was 21.082 ± 4.003 μg/g, which was within the effective concentration shown in Fig. 1 (1/4 to 1/16 Sr concentrations, 42 to 10.5 μg/ml). The concentration of Sr ions metabolized by blood absorption into the serums was 0.082 ± 0.003 μg/ml. With the extension of time, the concentrations of Sr ions in the hearts and serums gradually decreased to the level in the control group (fig. S8, A and B). To verify the biosafety of Sr ion composite hydrogels in vivo, we analyzed the concentrations of Sr ions in important organs and their metabolic pathways at different time points after injection. As expected, except increased

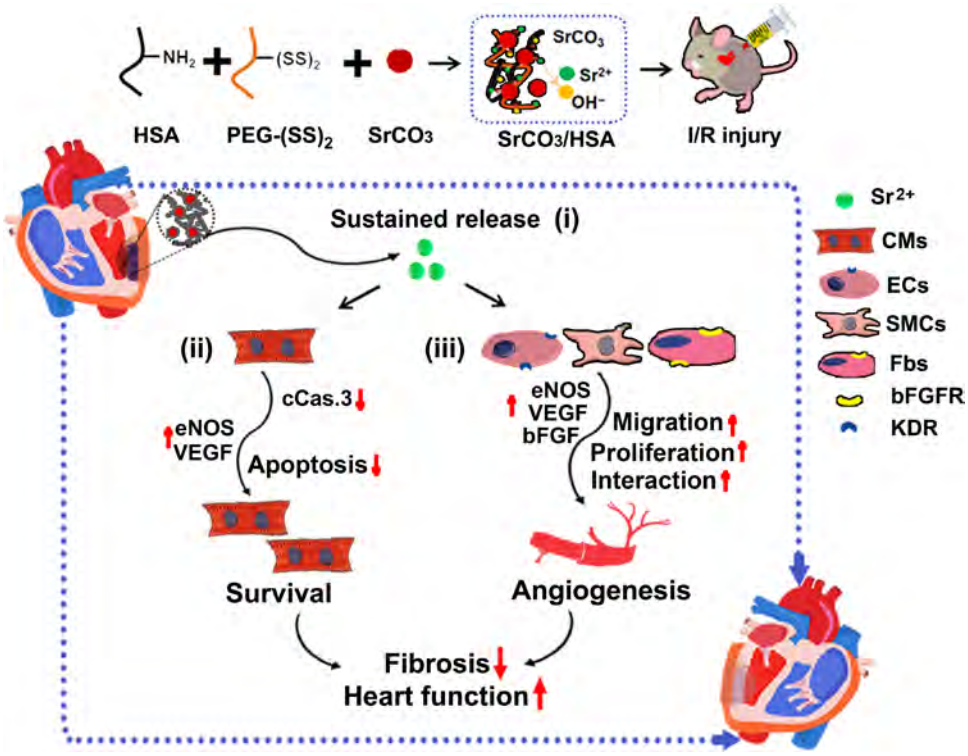

Fig. 7. The schematic diagram of the $SrCO_3$/HSA hydrogels in myocardium repair after I/R. Various underlying mechanisms contributed to myocardial repair for $SrCO_3$/HSA hydrogels after I/R: (**i**) $SrCO_3$/HSA hydrogels sustain the release of Sr ions in the infarct heart; (**ii**) Sr ions inhibit the apoptosis of CMs through reducing the activity of caspase-3; (**iii**) Sr ions promote angiogenesis via increasing proliferation, strengthening paracrine capacity, and stimulating the interaction of cardiac cells. Ultimately, alleviative fibrosis and elevated cardiac function are achieved after the treatment of $SrCO_3$/HSA hydrogels. ECs, endothelium cells; SMCs, smooth muscle cells; Fbs, fibroblasts.

concentrations in metabolites, such as urines and feces, but the Sr ion level in the urines was significantly higher than that in the feces ($P = 0.007$ and $P = 0.035$ at days 1 and 7, respectively) (fig. S8, C and D), there were no significant accumulations in other important organs, such as livers, kidneys, and lungs (fig. S8, E to G). The levels of Sr ions in serums, urine, and feces were increased during the first 7 to 14 days and then returned to normal levels at 28 days after injection, indicating that Sr ions are mainly excreted through urine metabolism and a few were metabolized through feces.

For application of a new biodegradable material, it is important to investigate its degradation profile in vivo. Therefore, we further studied the degradation of $SrCO_3$/HSA composite hydrogels in vivo after injected into the mice heart after I/R. The in situ $SrCO_3$ powders were detected by scanning electron microscope at days 1, 7, and 14 after I/R. As expected, the visible $SrCO_3$ powders in the cardiac tissue were gradually decreased with time, and no residual $SrCO_3$ particles were observed at day 14 after I/R. Besides, the mass percentage of Sr in heart tissue measured by energy dispersive spectrometer (EDS) analysis was significantly decreased and almost undetectable after 14 days (fig. S9A). Furthermore, the Western blot analysis reflected a similar degradation process of the HSA hydrogels, which were also almost completely degraded after 14 days (fig. S9, B and C). Those results indicate that the HSA hydrogel and $SrCO_3$ particles inside hydrogel were almost completely degraded simultaneously after 14 days.

Another critical issue for the clinical application of the $SrCO_3$/HSA composite hydrogels is their histotoxic effects on vital organs in vivo. To elucidate it, we conducted histopathological analyses of various organs (hearts, livers, spleens, lungs, and kidneys) in Sham mice at day 14 after injection of $SrCO_3$/HSA composite hydrogels (fig. S9D). Results showed that no $SrCO_3$ particles were observed in these organs and the treatment of $SrCO_3$/HSA composite hydrogels did not cause obvious structural abnormalities.

DISCUSSION

Myocardial ischemia is an enormous threat to public health and mostly caused by coronary artery thrombosis, which reduces or interrupts blood supply and leads to myocardial cell death (*28*). Recent studies have shown that intravenous injection of the solution containing Si ions could promote functional recovery and myocardial tissue repair after MI (*17*). However, it is not enough to only find the effective function of Si ions in the infarcted myocardium repair currently, and one of the key issues for bioactive ion therapy is to find an ion with stronger ability of promoting angiogenesis and cardiomyocyte survival. In the present study, using an in vivo I/R model and in vitro cell experiments, we reveal that Sr ions indeed have activity to improve the functional recovery and limit the fibrosis formation of ischemic hearts in vivo through enhancing angiogenesis and inhibiting cardiomyocyte apoptosis.

One of the important findings here is the determination of the bioactivity of Sr ions on cardiomyocyte. MI leads to cardiomyocyte apoptosis due to the insufficient blood supply, and inhibition of the cardiomyocyte apoptosis has been considered as one of effective treatments for MI (*29*, *30*). Similar to our recent discovery that Si

ions (4.53 to 9.08 μg/ml) have an antiapoptotic effect for NRCMs under glucose/oxygen-deprived conditions (*17*), our results show that Sr ions (10.59 to 42.36 μg/ml) play a protective role in the improvement of cell viability and decrease in the $TUNEL^+$ NRCMs treated under glucose/oxygen-deprived condition, accompanied with higher expression of cardiomyocyte marker genes after long-term coculture in vitro. Previous studies of Sr ions on cell viability mainly focus on bone and oral tissue repair, and the effect of Sr ions on cells are concentration dependent; in addition, low-dose Sr ions stimulate the viability of osteogenesis-related cells (2.19 to 43.81 μg/ml) (*31*) and reduce the apoptosis of human gingival cell (43.81 to 87.62 μg/ml) (*32*), but high-dose Sr ions inhibits the viability of osteogenesis-related cells (87.62 to 262.86 μg/ml) (*31*) and causes apoptosis in osteoclast (>788.56 μg/ml) (*33*). In the present study, we demonstrate that Sr ions have a significant protective effect on cardiomyocytes in a similar concentration range as that for enhancing viability of osteogenesis-related cells (*31*). Our study suggests that Sr ions are an activator of different types of cells including cells under stress such as hypoxic condition.

In addition, the recovery of blood perfusion is another critical issue for the repair of ischemic myocardial tissue (*19*). Reestablishment of blood flow in infarct tissue can provide sufficient oxygen and nutrients to cells in ischemic areas. One of the vital steps of angiogenesis is the proliferation and migration of endothelial cells and fibroblasts (*34*). Our results demonstrate that Sr ions indeed activate the early blood vessel formation by stimulating not only proliferation and migration of endothelial cells and fibroblasts but also the expression of angiogenic genes and protein in endothelial cells and fibroblasts. Besides sprouting capillary, the development and maturation of collateral coronary arteries are also essential for recovery and maintenance of sufficient blood flow, where the smooth muscle cells play a pivotal role in increasing the vessel capacity and reducing the fluid shear stress (*23*). Moreover, the regeneration of smooth muscle cells is essential for repair of ischemic hearts (*35*), and the expression of early proliferation–related genes of smooth muscle cells such as *C-FOS*, *C-MYC*, *C-SIS*, and *EGR-1* is critical for the activity of smooth muscle cells (*36*). Our results further confirm that Sr ions can facilitate the proliferation and migration of smooth muscle cells, as well as the expression of proliferation-related genes, suggesting that Sr ions may have a promotion effect on the formation of arteriole network by stimulating smooth muscle cells to support vascular integrity in structure and function. Besides focusing on the effects of bioactive ions on early angiogenesis, our results further revealed that Sr ions promote the formation of collateral coronary arteries by activating smooth muscle cells during the tissue repair process.

Cardiac tissue is composed of a multicellular microenvironment, and the cell-cell interaction is critical for tissue regeneration (*37*). The complex environment in vivo affects various cardiac cells. Therefore, the investigation of Sr ions simultaneously treating different cardiac cells is important to understand the therapeutic mechanisms of Sr ions. We find that Sr ions are able to not only activate a single type of cells but also activate the interaction between cardiomyocytes and endothelial cells, along with endothelial cells and fibroblasts. All these synergistic effects ultimately stimulate strengthening of the vascular ring formation of endothelial cells when cultured with NRCMs or HDFs in company with Sr ions. During the development of artery, the smooth muscle cells have connection and signal transmission with endothelial cells or extracellular matrix, which is involved in normal osmotic maintenance, vascular morphology support, and functional regulation (*38*). Therefore, the interactions between smooth muscle cells and endothelial cells play a key role in the process of arteriogenesis. Note that Sr ions can not only stimulate the paracrine effects between cells in promoting neovascularization but also stimulate the paracrine effects between smooth muscle cells and endothelial cells. As evidenced by preclinical studies, knockdown of the *PDGFB* gene causes pericyte depletion, and knockdown of *PDGFR* has the same effect (*39*). Our results reveal that Sr ions promote the expression of *PDGFB* from cocultured endothelial cells, and *PDGFB* further acts on the smooth muscle cells via *PDGFB* to induce the expression of early proliferation–related genes of smooth muscle cells lastly resulting in the maturation of neovascularization (*39*). Previous studies have shown that intercellular cross-talk among osteoblast, osteoclast, osteocyte, and chondrocyte is involved in the precise control of bone homeostasis, and Sr ions play a dual role in bone regeneration, on the one hand promoting osteogenesis and on the other hand inhibiting osteoclastogenesis (*40*). In our study, we demonstrate that the cross-talk between cardiomyocytes and blood vessel–forming cells is activated by Sr ions. Considering the multicell environment in cardiac tissue and the multistep processes in angiogenesis, it is advantageous for Sr ion–mediated cardioprotection, in which Sr ions seem to be a universal activator for different types of cells including vessel-forming cells (endothelial cells, fibroblasts, and smooth muscle cells) and cardiomyocytes, unlike the traditional biological approach for stimulating vessel formation, in which often one growth factor is applied and mainly stimulate certain kinds of cells with a specific receptor (*41*).

Although cell experiments in vitro have confirmed that Sr ions can activate cardiomyocytes and vascular cells, the effective delivery of Sr ions in situ and the long treatment time after injection are required for the myocardial repair after I/R. Therefore, it is critical to design biomaterials capable of sustainably releasing the Sr ions at appropriate concentration. We therefore design an injectable $SrCO_3$/HSA composite hydrogel, in which the controlled release of Sr ions is achieved. Because HSA is one of the most abundant proteins in human plasma, it has been used as an ideal drug carrier for its good biodegradability, low toxicity, and low immunogenicity (*42*). It has been shown that the free amino side chains of lysine residues on the surface of albumin can react with modified PEG-PEG [PEG-$(SS)_2$] to form amide bonds, which results in the formation of albumin hydrogels. At the same time, the active succinimide ester can react with the amino group on the surface of the tissue with good adhesion. Besides, the cross-linking reaction between the succinimide active ester of modified PEG and the free amino group of albumin occurs between pH 7.0 and pH 10.5 (*24*). Therefore, the alkaline environment generated by the hydrolysis of $SrCO_3$ can accelerate the process of gelation. The $SrCO_3$/HSA composite hydrogel is therefore selected, in which it releases Sr ions in an appropriate concentration range to reach the damaged zone of the tissue and creates alkaline environment to regulate the gelling time of the hydrogel. Our results show that the composite hydrogels have a sustained and stable release profile of Sr ions, indicating that the release of Sr ions from the hydrogels has long-term stability and maintains the effective concentrations for long-term treatment.

To verify the effects of Sr ions on the infarcted heart and answer the fundamental scientific question "whether bioactive Sr ions promote myocardial repair post-I/R in vivo," we inject $SrCO_3$/HSA composite hydrogels into the mice myocardium after 20 min after

I/R and evaluate the heart function over the 28 days after treatment. The results demonstrate that $SrCO_3$/HSA composite hydrogels significantly promote the recovery of cardiac function, reduce scar area at infarcted myocardium, and then decrease the degree of myocardial injury after I/R, which probably benefit from enhanced neovascularization and inhibition of cardiomyocytes apoptosis (*30*). Moreover, consistent with the in vitro results of Sr ions in promoting the proliferation, migration, and interaction of endothelial cells and smooth muscle cells, we observe significant increases in capillaries and arterioles in the mice heart treated with $SrCO_3$/HSA composite hydrogels, which is the first to verify the ability of Sr ions to induce the formation of both capillaries and normal collateral coronary arteries during the heart repair after I/R.

Considering that Sr ions improve the fibroblast proliferation, which plays an important role in regulating local fibrosis and extracellular matrix production during the wound healing (*27*), we also investigate the activation and viability of resident cardiac fibroblasts and myofibroblasts. We find that the Sr ions only enhance the proliferation of inactivated fibroblasts but not stimulate myofibroblast differentiation and activation. After infarction injury, fibroblasts and cardiomyocytes are partially killed within the ischemic area, and the remaining fibroblasts are activated to proliferate within 2 to 4 days to invade the necrotic area, followed by differentiation into myofibroblasts 3 to 7 days after injury to secrete abundant extracellular matrix proteins (*43*). Then, the scar forms to prevent ventricular wall thinning and rupturing. Our results show that Sr ions promote the proliferation of fibroblasts but do not stimulate myofibroblast differentiation and myofibroblast growth, which is necessary for both adaptive healing (*44*). These results suggest that Sr ions only enhance the repair of heart tissue damage by regulation of fibroblast proliferation but do not activate myofibroblasts and promote fibrosis. These beneficial effects may contribute to the repair of damaged heart tissues and recovery of heart function. In previous studies, Sr ions are mainly used in the field of bone tissue repair including the use of Sr ion–containing biomaterials as bone defect implants (*45*). Recently, a study reveals the activity of strontium-substituted bioglass for wound healing application, implying possible application for soft tissue therapy (*46*). Our study is the first to demonstrate the beneficial effects of Sr ion–containing biomaterials in promoting cardiac repair.

The delivery of Sr ions in the present study is facilitated using an HSA hydrogel. Injectable hydrogels have been used extensively as delivery systems of therapeutic agents for cardiac tissue engineering (*47*), in which the hydrogels are mainly functioning as carriers. On the other hand, some studies also show that some natural material–derived hydrogels, such as extracellular matrix, collagen, hyaluronic acid, and alginate-chitosan composite (*48*–*51*), have therapeutic effects on infarcted heart damage possibly through enhancing angiogenesis, cell recruitments, and differentiation, although the related mechanisms have not yet been fully explained. HSA hydrogels have been used for lung surgery and skin wound healing (*24*, *52*), but no studies on cross-linked pure HSA hydrogels for the treatment of MI have been reported. In addition, although the chemical-modified HSA solution as a donor of nitric oxide has been used in ischemic heart repair, the pure natural HSA solution does not show benefits for heart repair (*53*, *54*). In our study, we demonstrate that the cross-linked pure HSA hydrogel does not show bioactive effects but has good biocompatibility, degradability, and injectability for encapsulating $SrCO_3$ particles for Sr ion delivery, and only the $SrCO_3$/HSA composite hydrogel with Sr ion release property reveals specific activity in inhibiting cardiomyocyte apoptosis and enhancing angiogenesis in the infarcted hearts.

Regarding the effective application of Sr ion–containing hydrogels, the key to achieve effective treatment is whether the active concentration of Sr ions released by composite hydrogels is reached in vivo. By measuring the concentrations of Sr ion in the heart tissues, we identify that the initial concentrations of Sr ions in the hearts following hydrogel injection are within the effective range (10 to 42 μg/ml obtained from our in vitro cell experiments) and maintain within this effective range for 7 days. In contrast to the treatment of $SrCO_3$/HSA composite hydrogels, the Sr ion concentration in the heart and serum of the mice treated with the intramyocardial injection of Sr ion solution does not increase as compared with those in the control group 1 day after injection. Meanwhile, the heart function of the mice treated with Sr ion solution does not show significant improvement after I/R. These findings further confirm that the therapeutic function of the Sr ion composite hydrogels should be attributed to the prolonged release of bioactive Sr ions. Furthermore, with long-term treatment time (28 days), the concentrations of Sr ion in hearts gradually decrease to the normal level due to the metabolism. Moreover, the distributions of Sr ions in serums, feces, and urines are similar, with a clear increase in the early stage of the treatment (within 7 days), followed by a decrease to the normal level at the end of the treatment (28 days). Urines seem to be the main excretion way of Sr ions, which is consistent with previous literature reports (*55*), and other ions, such as Si ions (*17*), via the kidney irrespective of the route of administration. Since Sr ions are released into the body, biosafety is also a critical issue for clinical application. On the basis of it, we analyze the concentrations of Sr ion in some important organs. Our results show no accumulation of Sr ions in the important organs such as hearts, livers, kidneys, and lungs after 28 days of myocardial injection after I/R. Moreover, we also evaluate the histotoxic effects of myocardium injection with $SrCO_3$ composite hydrogels to several important organs (hearts, livers, spleens, lungs, and kidneys) in Sham mice, and no accumulation of particles or significant microstructure variation in the vital organs is observed 14 days after injection, which suggests that $SrCO_3$ composite hydrogels have good biosafety and no histopathological toxicity. Considering that the $SrCO_3$ particles are wrapped in HSA hydrogels when injected into the myocardium and the in vitro and in vivo degradation experiments prove the similar degradation rate of HSA hydrogels, $SrCO_3$/HSA hydrogels, and $SrCO_3$ particles inside the HSA hydrogels, which are consistent with the in vivo Sr ion metabolism results and other report about the degradation rate of HSA hydrogel (*52*), it is reasonable to suppose that $SrCO_3$ particles are mainly degraded together with the hydrogel matrix and hardly released to myocardial tissue or get into blood circulation to cause tissue toxicity. However, further studies are needed to confirm whether the micron-sized $SrCO_3$ particles will be degraded to the nanoscale and enter the blood circulation.

Previous literatures have also shown that the therapeutic method based on bioactive ions is more conducive to clinical transformation than the therapies of organic drugs, cell transplantation, recombinant proteins, and genetic engineering, since it has lower cost, higher stability, potentially greater safety, and varied methods of administration (*13*). Strontium ranelate, a drug containing Sr ions, has been used in the clinical treatment of osteoporosis and has recently shown positive effects in the treatment of knee osteoarthritis (*56*). However, a routine European Medicines Agency assessment of the benefit-risk

profile of strontium ranelate finds increased risk of serious MI with the use of strontium ranelate (*57*), but subsequent clinical studies reach the opposite conclusions, which reveal that there is no significant association between the use of strontium ranelate and the risk of MI (*57*). Our results also provide the role of Sr ions in MI from another perspective and show that the cardiac function of infarct mice can be improved by Sr ions to some extent at the appropriate concentration (HSA + 1% $SrCO_3$). Moreover, the Sr ions do not accumulate in the important organs and cause tissue toxicity. Meaningfully, our studies provide a further guide for the use and research of this kind of drugs from different aspects.

Note that we verify the role of $SrCO_3$/HSA composite hydrogels in promoting infarcted myocardium repair in vivo through a small animal, mouse heart I/R model. In the future, experimental models of larger animals should further explore the beneficial effects of hydrogels in vivo. Further studies can also focus on the molecular biological mechanisms by which Sr ions act in the post-I/R heart.

In summary, our study demonstrates that Sr ions are able to protect cardiomyocytes and promote blood vessel activation. On this basis, the Sr ion activity for promoting cardiac repair of infarcted hearts is further confirmed by the injection of designed $SrCO_3$/HSA composite hydrogels in a murine I/R mode. Furthermore, in vitro cell experiments verify the beneficial effect of Sr ions on cardiomyocyte survival and vascular cell proliferation, migration, and main angiogenesis–related gene expression. Last, reciprocal action between various cardiac cells, which is related to blood vessel formation and maturation, is proved to be activated after cell coculture, and their cell-cell interaction can be promoted after Sr ion treatment through intercellular paracrine action (Fig. 7). All these findings suggest that Sr ions have the potential to be a therapeutic element for impaired cardiac tissues when locally applied in the infarcted myocardium, which may provide a new therapeutic strategy, partly with superior practicability due to the ions' low cost, stability, biosecurity, and diversity, for the treatment of ischemic heart disease.

MATERIALS AND METHODS

Sr ion extract preparation and ion concentration determination

According to ISO/EN 10993-12, the extracts containing Sr ions were prepared by soaking SrO powder in serum-free Dulbecco's modified Eagle's medium (DMEM; Gibco) at a solid/liquid ratio of 200 mg/ml and incubated at 37°C for 24 hours. The mixture was centrifuged at 4000 rpm for 10 min, and then the supernatant was sterilized through a filter membrane (Millipore; 0.22 μm) and collected to obtain stock solutions. The concentrations of Sr ion in the stock solutions were measured using inductively coupled plasma optical emission spectroscopy (ICP-OES; 710-ES, Varian, USA). The stock extracts were diluted at the concentration of 170 μg/ml by cell growth medium and served as "1," and then the serial dilutions of extracts (1/2, 1/4, 1/8, 1/16, 1/32, 1/64, 1/128, and 1/256) were prepared by cell growth medium and stored at 4°C for future use. ICP-OES was used to determine the concentrations of the Sr ion in the solution. The cell growth medium without the addition of Sr ions was also analyzed by ICP-OES as the control group.

Cell isolation and culture

Neonatal Sprague-Dawley (SD) rats at the day of birth were purchased from Shanghai SLAC in Laboratory Animal Co. Ltd. (China). NRCMs were isolated from the SD rat hearts using a reported method (*17*). Briefly, the rats were anesthetized with isoflurane and euthanized by cervical dislocation, and their hearts were quickly removed. Left ventricles were collected and washed. After being dissected into pieces of <1 mm^3, the heart tissue was enzymatically dissociated into a single-cell suspension. The cell suspension was preplated for 2 hours to purify the cardiomyocytes. Then, the unattached cells were collected for further use. Primary NRCMs were used in this study. Cells were cultured with DMEM/F12 supplemented with 10% fetal bovine serum (FBS) and 1% P/S (penicillin/streptomycin) in a humid atmosphere of 5% CO_2 at 37°C. The culture medium was changed every other day.

HUVECs were isolated from the human umbilical cord vein as previously reported (*20*) and cultured with endothelial cell medium (ECM; ScienCell, USA) supplemented with 5% FBS and 1% endothelial cell growth supplement/heparin kit (ScienCell, USA). HUVECs below passage 5 were used in this study.

HUVSMCs were purchased from ScienCell company and cultured with smooth muscle cell medium (SMCM; ScienCell, USA) supplemented with 2.5% FBS and 1% smooth muscle cell growth supplement/heparin kit (ScienCell, USA). HUVSMCs below passage 3 were used in this study.

HDFs were isolated and cultured from the superficial layer of adult human skin dermatomes at a depth of 400 μm according to previous work (*20*) and cultured with DMEM/high glucose supplemented with 10% FBS and 1% P/S. HDFs below passage 10 were used for all studies.

HSFs were isolated from human hypertrophic scar tissue specimens according to previous work (*58*) and cultured with DMEM/high glucose supplemented with 10% FBS and 1% P/S. HSFs at lower than passage 6 were used for all studies.

Ventricular tissues were excised from male C57/B6 mice, rinsed with cold phosphate-buffered saline (PBS), minced with sterile fine scissors, and then placed in a 35-mm dish for enzymatic digestion (800 U/ml of Worthington collagenase type II in DMEM with equal proportion of 0.25% trypsin) as previously described (*59*). AMVFs were collected by centrifugation of the digestion solution, and cells were maintained in DMEM supplemented with 10% FBS and 1% P/S. AMVFs were then passaged once to passage 1 and plated at a density of 4×10^4 every well for further assays. Equilibration of cells in low-serum medium (0.1% FBS) was carried out for 6 hours before all treatments including recombinant TGF-β1 (10 ng/ml; Novoprotein, CA59) and Sr^{2+} (21 μg/ml) in DMEM. After culturing for 24 or 48 hours, the expression of α-SMA was detected though qRT-PCR and immunofluorescence.

Cell coculture

Direct contact coculture

In the NRCM (HUVSMCs or HDFs)–HUVEC direct contact coculture experiment, NRCMs (HUVSMCs or HDFs) were first seeded at a density of 2×10^4 cells/cm^2 in a six-well plate and cultured with control medium. After 24 hours, the HUVECs were seeded on the NRCMs (HUVSMCs or HDFs) at a density 2×10^4 cells/cm^2. After 12 hours, the culture medium was replaced by Sr ion–containing medium and continued culturing for 3 days. NRCMs (HUVSMCs or HDFs) and HUVECs were both mono-seeded at a density of 2×10^4 cells/cm^2 in a six-well plate. Monocultured NRCMs, HUVSMCs, HDFs, and HUVECs were cultured with DMEM/F12, SMCM, DMEM, and ECM, respectively. The medium for coculture is mixing DMEM/F12 (SMCM or DMEM) with ECM in equal proportion.

Indirect contact cocultures

In the NRCM (HUVSMCs or HDFs)–HUVEC indirect contact coculture experiment, the conditioned medium collected from NRCMs, HUVSMCs, and HDFs was used to culture HUVECs, and the conditioned medium collected from HUVECs was used to further culture NRCMs, HUVSMCs, and HDFs, respectively. Briefly, cells in an indirect coculture system, such as NRCMs, HUVSMCs, HUVECs, and HDFs, were seeded in six-well culture plate at a density of 2×10^4 cells/cm^2. After 24 hours, the culture medium was changed with Sr ion–containing medium, and the medium for indirect contact coculture of different types of cells was mixing DMEM/F12 (SMCM or DMEM) with ECM in equal proportion. At the same day, the other types of cells in an indirect coculture system were seeded in six-well culture plate at a density of 2×10^4 cells/cm^2. After the first seeded cells had been cultured with Sr ion–containing medium for 24 hours, the culture medium was collected and referred to as conditioned medium. Then, the conditioned medium was centrifuged at 1000 rpm/min for 5 min, and 3 ml of the supernatant was directly used to replace the medium from the other cells in an indirect coculture system and continue culturing for 3 days.

CCK8 analysis

The cells (HUVECs/HDFs/HUVSMCs/HSFs) were seeded on the 96-well plates at a density of 3×10^3 cells/cm^2 and cultured in a humidified incubator containing 5% CO_2 at 37°C. The number of parallel samples was six. After 12 hours of culture, the culture medium was replaced by the prepared culture medium containing diluted Sr ions at different concentrations (the concentration of Sr ions for HSFs was 1/8 dilution of the extracts). Then, the cells were cultured for 7 days with the medium daily changed, and a CCK8 assay (Beyotime) was applied on cells at days 1, 3, and 7 (or 5) according to the manufacturer's instruction. In addition, the NRCMs were seeded on the 96-well plates at a density of 1.5×10^4 cells/cm^2, and the viability of NRCMs treated with or without Sr ions after OGD injury was also measured by CCK8 assays as previously reported (*60*). Briefly, the culture medium was discarded at each time point, and the fresh culture medium containing CCK8 reagent (10:1) was added and cultured at 37°C for another 2 hours. Then, the absorbance of the as-mentioned medium was detected using a microplate reader (Synergy 2, BioTek) at a wavelength of 450 nm.

Ki67 immunofluorescent staining

The cells after culturing in the medium with or without Sr ions for 7 days were first fixed with 4% paraformaldehyde, permeabilized with 0.2% Triton X-100 (Sinopharm Chemical Reagent Co. Ltd., China) in PBS for 20 min, and blocked with 3% bovine serum albumin (BSA; Sangon Biotech, China) in PBS at room temperature for 30 min. Then, the cells were incubated in the first antibody reagent overnight at 4°C, followed by incubation in Alexa Fluor 594 immunoglobulin G (IgG) [heavy and light chains (H&L)] (1:500) and Alexa Fluor 488 IgG (H&L) (1:500) for 1 hour at room temperature. The samples were then rinsed with PBS, further stained with DAPI (4′,6-diamidino-2-phenylindole), and imaged using a confocal microscopy. The first antibody used in this study included anti-Ki67 (Abcam, ab16667), anti-CD31 (Abcam, ab28364), anti-vimentin (Abcam, ab8978), and anti–α-SMA (Abcam, ab5694). The cell staining was visualized using a Leica confocal microscope, and the number of Ki67$^+$ cells was counted using ImageJ software to calculate the proportion of Ki67$^+$ cells. Three duplicate samples were performed, and at least 10 independent sites of each sample were calculated.

Cell migration detection

The wound healing assay was performed as reported (*30*). The cells were seeded on six-well plates and cultured until confluence. Then, the cell monolayer was scrapped using a p200 pipette tip. After washing twice with PBS, the cells were cultured for 26 hours at 37°C with low-serum medium containing Sr ions (the time was recorded as 0 hours), which was the same as the total medium, except the FBS content was 0.5 volume %. The cells cultured with control medium without Sr ions were used as the control group. The optical images of each well were taken using an optical microscope at 0 hours. At 26 hours, the cells were fixed and stained with crystal violet, and the optical images of each well were taken using an optical microscope. The proportions of the initial scratch (A_0) and final scratch (A_1) were calculated using an ImageJ software program [National Institutes of Health (NIH)]. The migration ratio (A) was obtained by the following equation: $A = (A_0 - A_1)/A_0 \times 100\%$.

qRT-PCR analysis

For monocultured cells, HUVECs, HDFs, and HUVSMCs were cultured for 3 days with or without Sr ion treatment, while NRCMs were cultured for 10 days with or without Sr ion treatment; then, the cells were detached and centrifuged at 1000 rpm for 5 min and resuspended in TRIzol reagent (Invitrogen, Carlsbad, USA). For the analysis of AMVF activation, the cells were collected after 1 day of treatment. The complementary DNA (cDNA) was synthesized using a PrimeScript RT reagent kit (Takara Bio, Shiga, Japan), and highly purified primers used in this experiment were commercially synthesized (Shenggong Co. Ltd., Shanghai, China). The sequences of primers are listed in table S2. Quantification of all cDNA was carried out using a Bio-Rad MyiQ single-color real-time PCR system (*60*). All experiments were performed in triplicate to obtain average data.

For direct cocultured cells, they were harvested by trypsin, and HUVECs were then isolated from NRCMs/HUVSMCs/HDFs by applying magnetic beads coupled with an antibody against CD31, a specific protein of endothelial cells, according to the instructions (STEMCELL Technologies). The separated NRCMs, HUVECs, HUVSMCs, and HDFs were named Co-NRCMs, Co-HUVECs, Co-HUVSMCs, and Co-HDFs, respectively. For indirect cocultured cells, they were harvested by trypsin. Then, the process of the qRT-PCR assay was the same as the above description.

Protein isolation and Western blot analysis

After treatment for 5 days with or without Sr ions, the cells were rinsed with cold PBS and lysed for 15 min with radioimmunoprecipitation assay lysis buffer (Beyotime, Nantong, China) supplemented with protease and phosphatase inhibitors (Sigma Chemical Co., St. Louis, MO) in ice bath and isolated according to the standard protocol. Protein concentrations were analyzed by the bicinchoninic acid method. Each sample (50 μg of protein per lane) was separated by SDS–polyacrylamide gel (10%) electrophoresis, and the separated proteins were electrophoretically transferred from gel to a nitrocellulose membrane. Afterward, the membranes were immersed in blocking buffer for 1 hour at room temperature, followed by incubation with primary antibodies at 4°C overnight. Primary antibodies used here included anti-VEGF (Abcam) and anti–C-FOS (Abcam). The results were normalized by running parallel Western blot for detecting glyceraldehyde 3-phosphate dehydrogenase protein (GAPDH) (*17*).

vWF immunofluorescent staining

After being cultured on coverslips in the medium with Sr ions for 7 days, the coverslips were taken out of the wells, and the cell layers were washed three times with PBS and fixed with 4% (w/v) paraformaldehyde at 4°C for 20 min. Cells were then permeabilized with methanol and blocked with PBS containing 1% (w/v) BSA for 1 hour at 37°C before incubation in a primary antibody solution containing rabbit anti-vWF (diluted in PBS–0.5% BSA at 1/100) at 37°C for 2 hours. Then, cells were washed with PBS, followed by incubation with Alexa Fluor 488 goat anti-rabbit IgG secondary antibody (Invitrogen). Last, nuclei were revealed by incubating the cells with DAPI (1 μg/ml; FluoProbes) for 10 min at room temperature. The coverslips were then mounted on slides, the cells were observed with a fluorescence microscope (Leica DMI 3000B, Germany), and images were taken by a charge-coupled device camera (Leica DFC 420C). Ten images were taken per well, and for vWF, tubules were manually counted and averaged over the 10 images.

Cell model of OGD and TUNEL analysis

NRCMs were subjected to hypoxia in vitro in an oxygen control cabinet (Thermo Fisher Scientific, 51030287), which could use a mixture of 95% nitrogen, 1% hydrogen, and 5% CO_2 to create hypoxia. The NRCMs were treated with OGD by culturing in the culture medium without serum and glucose and under hypoxic condition (<1% O_2) for 4 hours as reported. Then, the medium was changed into normal culture medium with or without Sr ions, and the cell viability and apoptosis were analyzed 3 days later (*17*). Apoptotic cell observation was detected by TUNEL staining. Specifically, the cells were fixed in 4% paraformaldehyde and using the one-step TUNEL Apoptosis Assay Kit (Beyotime, Jiangsu, China) according to the manufacturer's protocol. The specific marker Cardiac Troponin T (cTnT) for the NRCMs was stained according to the above protocol. Cells were counterstained with DAPI (Sigma-Aldrich, St. Louis, MO, USA), and $TUNEL^+$ cells were observed by a fluorescence microscope (Leica DMI8, Germany). Total nuclei (DAPI staining, blue) in the NRCMs (cTnT staining, red) and $TUNEL^+$ nuclei (green) in each field were counted in 10 randomly chosen fields, and the index of apoptosis (number of $TUNEL^+$ nuclei/total number of nuclei × 100%) was calculated.

Preparation of $SrCO_3$/HSA composite hydrogels

First, HSA solution was prepared through mixing HSA solution (20 weight %; Yuanda Shuyang Pharmaceutical, Sichuan, China) with NaH_2PO_4 and Na_2HPO_4 powders to adjust the pH at 7.40. Then, 104 mg of PEG-$(SS)_2$ (JenKem Technology, Tianji, China; lot number: ZZ312P017, MW3500) was dissolved in 1 ml of PBS and mixed with HSA solution with equal volume proportion. The formed hydrogel was designated as HSA hydrogel (*24*). When preparing $SrCO_3$/HSA composite hydrogels, different amounts of $SrCO_3$ powders (Sinopharm, Beijing, China) were mixed thoroughly with 1 ml of HSA solution, followed by addition of 1 ml of PEG-$(SS)_2$ solution to form composite hydrogels with different $SrCO_3$ contents. In addition, the hydrogels with different weight volume ratios of $SrCO_3$ powders were designated as 0.5, 1, and 2% $SrCO_3$/HSA composite hydrogels. The particle size distribution of the $SrCO_3$ powders was analyzed using a laser particle size analyzer (Bettersize2600, Bettersize Instruments Ltd., China).

Determination of the optimal $SrCO_3$/HSA composite hydrogels

The hydrogels were incubated in serum-free DMEM at 37°C, and the hydrogel/medium volume fraction was 1/1.5. We changed the medium every other day and collected the replaced medium for concentration determination. After 1, 3, 5, 7, and 9 days of incubation, the concentrations of Sr ion in the medium were measured by ICP-OES. The number of parallel samples was three.

Determination of the gelation time of hydrogels

The gelation time of composite hydrogels was determined according to the method described in a previous report (*24*). Briefly, 1 ml of freshly made PEG-$(SS)_2$ solution was poured quickly into a 5-ml microcentrifuge tube containing 1 ml of HSA solution with or without different amounts of $SrCO_3$ powders. The tube was tilted every 5 s until the composite hydrogel was formed and did not change its position with the tilting vial. The relevant period of time was recorded as the gelation time, and three measurements were repeated for each sample.

Rheological characterization of hydrogels

Oscillatory amplitude sweeps and oscillatory frequency sweeps of HSA hydrogel and HSA + 1% Sr composite hydrogel were tested by an Anton Paar MCR 302 rheometer. For the oscillatory amplitude sweeps, each oscillatory measurement has been preceded by an oscillatory amplitude sweep test at a frequency of 1 rad/s with deformations ranging from 0.01 to 1000%. For the oscillatory frequency sweep test, the applied strain was 1%, while the shear frequency varied from 0.01 to 100 rad/s.

Degradation of hydrogels in vitro

To investigate the degradation of the HSA hydrogel, HSA + 1% Sr composite hydrogel, and $SrCO_3$ powders inside the HSA + 1% Sr composite hydrogel, the samples (HSA hydrogel and HSA + 1% Sr composite hydrogel) were soaked in tris-HCl buffer solution (pH 7.4) at 37°C in a shaking water bath for 1, 3, 5, 7, and 14 days. The ratio of tris-HCl buffer volume to the hydrogel was 10 ml/g. After different time periods (1, 3, 5, 7, and 14 days), the samples were freeze-dried for 24 hours and weighed, followed by calcination at 700°C for 3 hours. Then, the remaining $SrCO_3$ powders were lastly weighted. Three samples were used for each group for reproducibility.

Animals

Adult male C57 BL/6 mice (12 weeks old) were purchased from the Shanghai SLAC in Laboratory Animal Co. Ltd., Shanghai, China. Protocols were approved by the Institutional Animal Care and Use Committee of Shanghai Institute of Nutrition and Health, in accordance with the Guidelines for the Care and Use of Laboratory Animals published by the U.S. NIH (NIH publication, eighth edition, 2011).

Murine myocardial I/R model and hydrogel treatment

To induce I/R model, mice were subjected to left anterior descending (LAD) coronary artery ligation as described previously (*8*, *10*). Briefly, the animals were anesthetized using pentobarbital sodium (50 mg/kg) and ventilated using a rodent ventilator (DW-3000B) with 90 breaths/min and a stroke volume of 100 ml. The heart was exposed through a left-sided minithoracotomy, and 7-0 prolene suture was passed underneath the LAD at 2 to 3 mm distal to its origin between the left auricle and conus arteriosus. A suture loop around the artery was tightened to ensure the LAD occlusion, which was subsequently removed after 60 min to allow for reperfusion. Then, the mice were randomly divided into three groups: I/R + control, I/R + HSA, and I/R + HSA + 1% Sr. After all, 20 min later, a total

volume of 20 μl of HSA hydrogels, mixed with $SrCO_3$ powders, was injected into two sites (10 μl per site) in the border zones of infarcted myocardium for the I/R + HSA + 1% Sr group, and the equal amount of HSA hydrogels was injected into the mice heart in I/R + HSA group. The mice that received no injection were set as I/R + control group. Then, the animals were allowed to awaken on a warm pad and kept in a cage with free access to wet food and water during the reperfusion period. The mice in Sham group only underwent the same surgical procedure except for the ligation of LAD. The body weight was recorded at days 0, 1, 7, and 28 after I/R.

To compare the beneficial role of the sustained release of Sr ions from HSA + 1% Sr composite hydrogels in ischemic heart healing, the I/R mice were randomly divided into I/R, I/R + Sr^{2+} (21 μg/ml), and I/R + HSA + 1% Sr. Different components in a total volume of 20 μl were injected into the hearts 20 min after reperfusion, and the mice were maintained for the subsequent analysis.

Echocardiography

The cardiac function was analyzed at days 1 and 28 after I/R using transthoracic echocardiography as reported previously (*10*, *30*). Mice were anesthetized with inhalation of isoflurane (1 to 1.5%) in O_2, and their chest hair was removed using depilatory paste. M-mode echocardiography was performed with a vevo 2100 imaging system (VisualSonics Inc., Canada) with a 400-MHz transducer. The short-axis and long-axis views were obtained to measure the cardiac parameters. The percentage of LVEF and LVFS was detected.

LDH activity analysis

Measurement of LDH activity was performed according to the supplier's instructions (LDH Cytotoxicity Assay Kit, Beyotime Institute of Biotechnology). LDH activity in the LV serum at day 3 of reperfusion was measured. Briefly, the serum was collected from the blood supernatant, extracted from the LV cardiac cavity of anesthetized mice, and centrifuged at 3000 rpm for 10 min at 4°C. Then, 2 μl of each serum sample was transferred to another 96-well plate; 60 μl of reaction solution was then added into each well, and the plate was placed on a shaker for 30 min at room temperature. The release of LDH into the medium was measured by detecting the optical density at 490 and 600 nm using a microplate reader (Synergy HT; BioTek, Broadview, IL).

Western blot analysis

The heart was harvested at days 1, 3, 7, and 14 after I/R, and the LV tissue was dissected and stored at −80°C until being homogenized and digested in tissue lysis buffer (with protease and phosphatase inhibitors, Thermo Fisher Scientific). The resulting suspensions were centrifuged at 10,000*g* for 30 min at 4°C, and the protein supernatant was collected. Western blot analysis was performed following a previously described method (*10*), and the antibodies used for analysis were total/cleaved caspase-3 (Cell Signaling Technology, 9662s), VEGF (Servicebio, GB11034B), eNOS (Servicebio, GB11086), β-tubulin (Servicebio, GB13017), and human-specific HSA (Signalway Antibody, 27044).

Histological analysis

After being conducted with the final echocardiography, the mice were euthanized, and the hearts were harvested as reported previously (*30*). The heart tissues were washed by PBS, fixed for 1 hour at room temperature in 4% paraformaldehyde solution, and perfused with 30% sucrose at 4°C overnight before embedded in optimal cutting temperature compound (O. C. T.) for frozen section. Then, 5-μm sections were cut in a Leica CM1950 cryostat for Masson's trichrome staining and immunostaining analysis. Slices were stained with Masson's trichrome staining to detect the scar area in infarct hearts. The scar area and LV area were measured by ImageJ software. The degree of fibrosis was calculated as the ratio of scar area to LV area. The α-SMA, CD31, and VEGF immunofluorescence staining was performed to investigate the effect of $SrCO_3$/HSA composite hydrogels on angiogenesis and the level of angiogenic factors in vivo. Total α-SMA^+ round vessels, $CD31^+$ cells, and $VEGF^+$ area in each field were counted in 10 to 15 randomly chosen fields from five different heart slides in each group. The TUNEL staining was performed at day 3 after I/R to investigate the effect of $SrCO_3$/HSA composite hydrogels on myocardial apoptosis in vivo according to the kit manufacturer's instruction (Sigma-Aldrich), and the index of apoptosis (number of $TUNEL^+$ nuclei/total number of nuclei × 100%) was calculated. The protocol of the immunofluorescence staining for heart cryosections was the same as that of staining in cells in vitro. To visualize the overall tissue morphology and analyze the histotoxicity in the Sham mice after the treatment of $SrCO_3$/HSA composite hydrogels at day 14 after injection, the slices of hearts, livers, spleens, lungs, and kidneys were stained with Gill's 3 hematoxylin and aqueous eosin Y solution (Sigma-Aldrich).

Metabolism and distribution analyses

The metabolism of the biodegraded $SrCO_3$/HSA composite hydrogels after injection was investigated by determining the concentrations of Sr ion in serum, urine, and feces collected from the mice at days 1, 7, 14, and 28 after I/R. The accumulation and distribution of Sr ions in important organs such as heart, liver, kidney, and lung after I/R were also analyzed. The results were compared with the control group without the treatment of the $SrCO_3$/HSA composite hydrogels. The tissue samples were chemically digested in concentrated nitric acid (spectral purity) using a microwave digester, and the concentrations of Sr ion in the samples were determined by inductively coupled plasma mass spectrometry (ICP-MS; PerkinElmer NexION 350X, USA). In addition, the concentrations of Sr ions in hearts and cardiac serums collected from the mice injected with Sr ions alone at days 1 and 7 after I/R were also determined by ICP-MS (PerkinElmer NexION 350X, USA) as described above.

Degradation of the $SrCO_3$/HSA composite hydrogel in vivo

The hearts were harvested at days 1, 7, and 14 after I/R. Then, 20-μm slices were cut from the hearts embedded in O.C.T. for frozen sectioning in a Leica CM1950 cryostat, followed by vacuum freeze-drying for the observation of residual $SrCO_3$ after degradation. The scanning electron microscope microscopic observation and EDS element content analysis of the slices were conducted (S-4800, Hitachi, Japan). EDS analysis of Sr contents in heart tissues was obtained by calculating the mass percentage of Sr versus all detected elements such as C, O, and Sr. Moreover, the Western blot analysis was used to detect the HSA in heart tissues at different time points as described above.

Statistical analysis

Data are presented as means ± SEM from at least three independent experiments. Statistical significance between two groups was determined by Student's *t* test. Statistical significance among more than two groups was determined by one-way analysis of variance (ANOVA), followed by Bonferroni post hoc test. Two-way ANOVA was applied with Tukey's multiple comparison for analysis of echocardiographic

data. Statistical analyses were performed with GraphPad Prism software (version 6.1), and a P value of less than 0.05 was considered statistically significant.

SUPPLEMENTARY MATERIALS

Supplementary material for this article is available at http://advances.sciencemag.org/cgi/content/full/7/3/eabe0726/DC1

View/request a protocol for this paper from *Bio-protocol*.

REFERENCES AND NOTES

1. R. Zarrinkoub, B. Wettermark, P. Wändell, M. Mejhert, R. Szulkin, G. Ljunggren, T. Kahan, The epidemiology of heart failure, based on data for 2.1 million inhabitants in Sweden. *Eur. J. Heart Fail.* **15**, 995–1002 (2013).
2. A. Caccioppo, L. Franchin, A. Grosso, F. Angelini, F. D'Ascenzo, M. F. Brizzi, Ischemia reperfusion injury: Mechanisms of damage/protection and novel strategies for cardiac recovery/regeneration. *Int. J. Mol. Sci.* **20**, 5024 (2019).
3. J. Vinten-Johansen, Z.-Q. Zhao, R. Jiang, A. J. Zatta, G. P. Dobson, Preconditioning and postconditioning: Innate cardioprotection from ischemia-reperfusion injury. *J. Appl. Physiol.* **103**, 1441–1448 (2007).
4. S. M. Davidson, P. Ferdinandy, I. Andreadou, H. E. Bøtker, G. Heusch, B. Ibáñez, M. Ovize, R. Schulz, D. M. Yellon, D. J. Hausenloy, D. Garcia-Dorado; CARDIOPROTECTION COST Action (CA16225), Multitarget strategies to reduce myocardial ischemia/reperfusion injury: JACC review topic of the week. *J. Am. Coll. Cardiol.* **73**, 89–99 (2019).
5. Z. Q. Zhao, J. S. Corvera, M. E. Halkos, F. Kerendi, N. P. Wang, R. A. Guyton, J. Vinten-Johansen, Inhibition of myocardial injury by ischemic postconditioning during reperfusion: Comparison with ischemic preconditioning. *Am. J. Physiol. Heart Circ. Physiol.* **285**, H579–H588 (2003).
6. G. Zhang, S. Gao, X. Li, L. Zhang, H. Tan, L. Xu, Y. Chen, Y. Geng, Y. Lin, B. Aertker, Y. Sun, Pharmacological postconditioning with lactic acid and hydrogen rich saline alleviates myocardial reperfusion injury in rats. *Sci. Rep.* **5**, 9858 (2015).
7. M. V. Cohen, J. M. Downey, Signalling pathways and mechanisms of protection in pre- and postconditioning: Historical perspective and lessons for the future. *Br. J. Pharmacol.* **172**, 1913–1932 (2015).
8. G. de Couto, W. Liu, E. Tseliou, B. Sun, N. Makkar, H. Kanazawa, M. Arditi, E. Marbán, Macrophages mediate cardioprotective cellular postconditioning in acute myocardial infarction. *J. Clin. Invest.* **125**, 3147–3162 (2015).
9. K. Y. Zhu, Q. Wu, C. Ni, P. Zhang, Z. Zhong, Y. Wu, Y. Wang, Y. Xu, M. Kong, H. Cheng, Z. Tao, Q. Yang, H. Liang, Y. Jiang, Q. Li, J. Zhao, J. Huang, F. Zhang, Q. Chen, Y. Li, J. Chen, W. Zhu, H. Yu, J. Zhang, H.-T. Yang, X. Hu, J. Wang, Lack of remuscularization following transplantation of human embryonic stem cell-derived cardiovascular progenitor cells in infarcted nonhuman primates. *Circ. Res.* **122**, 958–969 (2018).
10. J. Wang, M. Liu, Q. Wu, Q. Li, L. Gao, Y. Jiang, B. Deng, W. Huang, W. Bi, Z. Chen, Y. E. Chin, C. Paul, Y. Wang, H.-T. Yang, Human embryonic stem cell-derived cardiovascular progenitors repair infarcted hearts through modulation of macrophages via activation of signal transducer and activator of transcription 6. *Antioxid. Redox Signal.* **31**, 369–386 (2019).
11. M. Qasim, P. Arunkumar, H. M. Powell, M. Khan, Current research trends and challenges in tissue engineering for mending broken hearts. *Life Sci.* **229**, 233–250 (2019).
12. H. Hashimoto, E. N. Olson, R. Bassel-Duby, Therapeutic approaches for cardiac regeneration and repair. *Nat. Rev. Cardiol.* **15**, 585–600 (2018).
13. V. Mouriño, J. P. Cattalini, A. R. Boccaccini, Metallic ions as therapeutic agents in tissue engineering scaffolds: An overview of their biological applications and strategies for new developments. *J. R. Soc. Interface* **9**, 401–419 (2012).
14. A. Hoppe, N. S. Guldal, A. R. Boccaccini, A review of the biological response to ionic dissolution products from bioactive glasses and glass-ceramics. *Biomaterials* **32**, 2757–2774 (2011).
15. Y. L. Zhou, C. T. Wu, J. Chang, Bioceramics to regulate stem cells and their microenvironment for tissue regeneration. *Mater. Today* **24**, 41–56 (2019).
16. X. T. Wang, L. Wang, Q. Wu, F. Bao, H. Yang, X. Qiu, J. Chang, Chitosan/calcium silicate cardiac patch stimulates cardiomyocyte activity and myocardial performance after infarction by synergistic effect of bioactive ions and aligned nanostructure. *ACS Appl. Mater. Inter.* **11**, 1449–1468 (2019).
17. M. Yi, H. Li, X. Wang, J. Yan, L. Gao, Y. He, X. Zhong, Y. Cai, W. Feng, Z. Wen, C. Wu, C. Ou, J. Chang, M. Chen, Ion therapy: A novel strategy for acute myocardial infarction. *Adv. Sci.* **6**, 1801260 (2019).
18. L. X. Mao, L. Xia, J. Chang, J. Liu, L. Jiang, C. Wu, B. Fang, The synergistic effects of Sr and Si bioactive ions on osteogenesis, osteoclastogenesis and angiogenesis for osteoporotic bone regeneration. *Acta Biomater.* **61**, 217–232 (2017).
19. C. Cochain, K. M. Channon, J. S. Silvestre, Angiogenesis in the infarcted myocardium. *Antioxid. Redox Signal.* **18**, 1100–1113 (2013).
20. H. Li, J. Chang, Bioactive silicate materials stimulate angiogenesis in fibroblast and endothelial cell co-culture system through paracrine effect. *Acta Biomater.* **9**, 6981–6991 (2013).
21. I. E. Hoefer, J. J. Piek, G. Pasterkamp, Pharmaceutical interventions to influence arteriogenesis: New concepts to treat ischemic heart disease. *Curr. Med. Chem.* **13**, 979–987 (2006).
22. U. Roostalu, B. Aldeiri, A. Albertini, N. Humphreys, M. Simonsen-Jackson, J. K. F. Wong, G. Cossu, Distinct cellular mechanisms underlie smooth muscle turnover in vascular development and repair. *Circ. Res.* **122**, 267–281 (2018).
23. U. K. Allahwala, L. M. Khachigian, D. Nour, A. Ridiandres, M. Billah, M. Ward, J. Weaver, R. Bhindi, Recruitment and maturation of the coronary collateral circulation: Current understanding and perspectives in arteriogenesis. *Microvasc. Res.* **132**, 104058 (2020).
24. Y. L. Zhou, L. Gao, J. Peng, M. Xing, Y. Han, X. Wang, Y. Xu, J. Chang, Bioglass activated albumin hydrogels for wound healing. *Adv. Healthc. Mater.* **7**, e1800144 (2018).
25. Z. Tao, B. Chen, X. Tan, Y. Zhao, L. Wang, T. Zhu, K. Cao, Z. Yang, Y. W. Kan, H. Su, Coexpression of VEGF and angiopoietin-1 promotes angiogenesis and cardiomyocyte proliferation reduces apoptosis in porcine myocardial infarction (MI) heart. *Proc. Natl. Acad. Sci. U.S.A.* **108**, 2064–2069 (2011).
26. Y. Azizi, M. Faghihi, A. Imani, M. Roghani, A. Zekri, M. B. Mobasheri, T. Rastgar, M. Moghimian, Post-infarct treatment with [Pyr^1]apelin-13 improves myocardial function by increasing neovascularization and overexpression of angiogenic growth factors in rats. *Eur. J. Pharmacol.* **761**, 101–108 (2015).
27. Y. Ma, R. P. Iyer, M. Jung, M. P. Czubryt, M. L. Lindsey, Cardiac fibroblast activation post-myocardial infarction: Current knowledge gaps. *Trends Pharmacol. Sci.* **38**, 448–458 (2017).
28. K. P. Rentrop, F. Feit, Reperfusion therapy for acute myocardial infarction: Concepts and controversies from inception to acceptance. *Am. Heart J.* **170**, 971–980 (2015).
29. D. Wencker, M. Chandra, K. Nguyen, W. Miao, S. Garantziotis, S. M. Factor, J. Shirani, R. C. Armstrong, R. N. Kitsis, A mechanistic role for cardiac myocyte apoptosis in heart failure. *J. Clin. Invest.* **111**, 1497–1504 (2003).
30. Q. Wu, J. Wang, W. L. W. Tan, Y. Jiang, S. Wang, Q. Li, X. Yu, J. Tan, S. Liu, P. Zhang, Z. Tiang, Z. Chen, R. S. Y. Foo, H. T. Yang, Extracellular vesicles from human embryonic stem cell-derived cardiovascular progenitor cells promote cardiac infarct healing through reducing cardiomyocyte death and promoting angiogenesis. *Cell Death Dis.* **11**, 354 (2020).
31. A. Aimaiti, A. Maimaitiyiming, X. Boyong, K. Aji, C. Li, L. Cui, Low-dose strontium stimulates osteogenesis but high-dose doses cause apoptosis in human adipose-derived stem cells via regulation of the ERK1/2 signaling pathway. *Stem Cell Res. Ther.* **8**, 282 (2017).
32. G. Fernandes, S. T. Vanyo, S. B. A. Alsharif, S. Andreana, M. B. Visser, R. Dziak, Strontium effects on human gingival fibroblasts. *J. Oral Implantol.* **45**, 274–280 (2019).
33. A. S. Hurtel-Lemaire, R. Mentaverri, A. Caudrillier, F. Cournarie, A. Wattel, S. Kamel, E. F. Terwilliger, E. M. Brown, M. Brazier, The calcium-sensing receptor is involved in strontium ranelate-induced osteoclast apoptosis. *J. Biol. Chem.* **284**, 575–584 (2009).
34. V. Siavashi, S. M. Nassiri, R. Rahbarghazi, Z. Mohseni, A. M. Sharifi, Distinct Tie2 tyrosine phosphorylation sites dictate phenotypic switching in endothelial progenitor cells. *J. Cell. Physiol.* **234**, 6209–6219 (2019).
35. A. Yanagisawa-Miwa, Y. Uchida, F. Nakamura, T. Tomaru, H. Kido, T. Kamijo, T. Sugimoto, K. Kaji, M. Utsuyama, C. Kurashima, H. Ito, Salvage of infarcted myocardium by angiogenic action of basic fibroblast growth factor. *Science* **257**, 1401–1403 (1992).
36. K. Ranganna, T. Joshi, F. M. Yatsu, Sodium-butyrate inhibits platelet-derived growth factor-induced proliferation of vascular smooth-muscle cells. *Arterioscl. Thromb. Vas.* **15**, 2273–2283 (1995).
37. C. Piard, A. Jeyaram, Y. Liu, J. Caccamese, S. M. Jay, Y. Chen, J. Fisher, 3D printed HUVECs/MSCs cocultures impact cellular interactions and angiogenesis depending on cell-cell distance. *Biomaterials* **222**, 119423 (2019).
38. R. A. Mathura, S. Russell-Puleri, L. M. Cancel, J. M. Tarbell, Hydraulic conductivity of endothelial cell-initiated arterial cocultures. *Ann. Biomed. Eng.* **42**, 763–775 (2014).
39. M. Hellstrom, M. Kalen, P. Lindahl, A. Abramsson, C. Betsholtz, Role of PDGF-B and PDGFR-beta in recruitment of vascular smooth muscle cells and pericytes during embryonic blood vessel formation in the mouse. *Development* **126**, 3047–3055 (1999).
40. Y. Zhang, G. Luo, X. Yu, Cellular communication in bone homeostasis and the related anti-osteoporotic drug development. *Curr. Med. Chem.* **27**, 1151–1169 (2020).
41. M. di Somma, M. Vliora, E. Grillo, B. Castro, E. Dakou, W. Schaafsma, J. Vanparijs, M. Corsini, C. Ravelli, E. Sakellariou, S. Mitola, Role of VEGFs in metabolic disorders. *Angiogenesis* **23**, 119–130 (2020).
42. F. Kratz, Albumin as a drug carrier: Design of prodrugs, drug conjugates and nanoparticles. *J. Control. Release* **132**, 171–183 (2008).
43. X. Fu, H. Khalil, O. Kanisicak, J. G. Boyer, R. J. Vagnozzi, B. D. Maliken, M. A. Sargent, V. Prasad, I. Valiente-Alandi, B. C. Blaxall, J. D. Molkentin, Specialized fibroblast differentiated states underlie scar formation in the infarcted mouse heart. *J. Clin. Invest.* **128**, 2127–2143 (2018).

44. O. Kanisicak, H. Khalil, M. J. Ivey, J. Karch, B. D. Maliken, R. N. Correll, M. J. Brody, S. C. J. Lin, B. J. Aronow, M. D. Tallquist, J. D. Molkentin, Genetic lineage tracing defines myofibroblast origin and function in the injured heart. *Nat. Commun.* **7**, 12260 (2016).
45. D. Pierantozzi, A. Scalzone, S. Jindal, L. Stīpniece, K. Šalma-Ancāne, K. Dalgarno, P. Gentile, E. Mancuso, 3D printed Sr-containing composite scaffolds: Effect of structural design and material formulation towards new strategies for bone tissue engineering. *Compos. Sci. Technol.* **191**, 108069 (2020).
46. S. Jebahi, H. Oudadesse, N. Jardak, I. Khayat, H. Keskes, A. Khabir, T. Rebai, H. el Feki, A. el Feki, Biological therapy of strontium-substituted bioglass for soft tissue wound-healing: Responses to oxidative stress in ovariectomised rats. *Ann. Pharm. Fr.* **71**, 234–242 (2013).
47. B. Peña, M. Laughter, S. Jett, T. J. Rowland, M. R. G. Taylor, L. Mestroni, D. Park, Injectable hydrogels for cardiac tissue engineering. *Macromol. Biosci.* **18**, e1800079 (2018).
48. S. B. Seif-Naraghi, J. M. Singelyn, M. A. Salvatore, K. G. Osborn, J. J. Wang, U. Sampat, O. L. Kwan, G. M. Strachan, J. Wong, P. J. Schup-Magoffin, R. L. Braden, K. Bartels, J. A. DeQuach, M. Preul, A. M. Kinsey, A. N. DeMaria, N. Dib, K. L. Christman, Safety and efficacy of an injectable extracellular matrix hydrogel for treating myocardial infarction. *Sci. Transl. Med.* **5**, 173ra25 (2013).
49. N. J. R. Blackburn, T. Sofrenovic, D. Kuraitis, A. Ahmadi, B. McNeill, C. Deng, K. J. Rayner, Z. Zhong, M. Ruel, E. J. Suuronen, Timing underpins the benefits associated with injectable collagen biomaterial therapy for the treatment of myocardial infarction. *Biomaterials* **39**, 182–192 (2015).
50. S. J. Yoon, Y. H. Fang, C. H. Lim, B. S. Kim, H. S. Son, Y. Park, K. Sun, Regeneration of ischemic heart using hyaluronic acid-based injectable hydrogel. *J. Biomed. Mater. Res. B Appl. Biomater.* **91**, 163–171 (2009).
51. B. Y. Deng, L. Shen, Y. Wu, Y. Shen, X. Ding, S. Lu, J. Jia, J. Qian, J. Ge, Delivery of alginate-chitosan hydrogel promotes endogenous repair and preserves cardiac function in rats with myocardial infarction. *J. Biomed. Mater. Res. A* **103**, 907–918 (2015).
52. H. Kobayashi, T. Sekine, T. Nakamura, Y. Shimizu, In vivo evaluation of a new sealant material on a rat lung air leak model. *J. Biomed. Mater. Res.* **58**, 658–665 (2001).
53. H. Li, L. Ma, C. J. Hsia, J. L. Zweier, P. Kuppusamy, Polynitroxyl-albumin (PNA) enhances myocardial infarction therapeutic effect of tempol in rat hearts subjected to regional ischemia-reperfusion. *Free Radic. Biol. Med.* **32**, 712–719 (2002).
54. S. Hallstrom, M. Franz, H. Gasser, M. Vodrazka, S. Semsroth, U. M. Losert, M. Haisjackl, B. K. Podesser, T. Malinski, S-nitroso human serum albumin reduces ischaemia/reperfusion injury in the pig heart after unprotected warm ischaemia. *Cardiovasc. Res.* **77**, 506–514 (2008).
55. H. Spencer, D. Laszlo, M. Brothers, Strontium^{85} and calcium^{45} metabolism in man. *J. Clin. Invest.* **36**, 680–688 (1957).
56. S. O'Donnell, A. Cranney, G. A. Wells, J. D. Adachi, J. Y. Reginster, Strontium ranelate for preventing and treating postmenopausal osteoporosis. *Cochrane Database Syst. Rev.* **19**, CD005326 (2006).
57. H. Svanstrom, B. Pasternak, A. Hviid, Use of strontium ranelate and risk of acute coronary syndrome: Cohort study. *Ann. Rheum. Dis.* **73**, 1037–1043 (2014).
58. M. Chang, X. Ma, T. Ouyang, J. Lin, J. Liu, Y. Xiao, H. Chen, J. Yu, Y. Huang, M. Xu, Potential molecular mechanisms involved in 5-aminolevulinic acid-based photodynamic therapy against human hypertrophic scars. *Plast. Reconstr. Surg.* **136**, 715–727 (2015).
59. M. S. Stratton, R. A. Bagchi, M. B. Felisbino, R. A. Hirsch, H. E. Smith, A. S. Riching, B. Y. Enyart, K. A. Koch, M. A. Cavasin, M. Alexanian, K. Song, J. Qi, M. E. Lemieux, D. Srivastava, M. P. Y. Lam, S. M. Haldar, C. Y. Lin, T. A. McKinsey, Dynamic chromatin targeting of BRD4 stimulates cardiac fibroblast activation. *Circ. Res.* **125**, 662–677 (2019).
60. M. Xing, X. Wang, E. Wang, L. Gao, J. Chang, Bone tissue engineering strategy based on the synergistic effects of silicon and strontium ions. *Acta Biomater.* **72**, 381–395 (2018).

Acknowledgments

Funding: This work was supported by the National Key R&D Program of China (2016YFC1100201, 2017YFA0103700, and 2016YFC1301204), the Strategic Priority Research Program of the CAS (XDA16010203 and XDA16010201), the National Natural Science Foundation of China (32000945, 51902335, 81520108004, and 81470422), and Shanghai Municipal Natural Science Foundation (19ZR1465200). **Author contributions:** J.C., H.-T.Y., M.X., and Y.J. designed the research. M.X. performed the in vitro experiments, analyzed the data, and drafted the paper. Y.J. performed in vivo experiments, analyzed the data, and drafted the paper. W.B. constructed the animal models. L.G. and Y.-L.Z. guided the preparation of materials. S.-L.R., L.-L.M., and Z.-W.Z. performed the AMVF isolation, culture, and treatment with TGF-β or Sr ions, hydrogel in vitro degradation, and HSF cell culture experiments, respectively. J.C. and H.-T.Y. directed the research, analyzed the data, revised and final approved the manuscript, and provided financial support. **Competing interests:** The authors declare that they have no competing interests. **Data and materials availability:** All data needed to evaluate the conclusions in the paper are present in the paper and/or the Supplementary Materials. Additional data related to this paper may be requested from the authors.

Submitted 30 July 2020
Accepted 20 November 2020
Published 15 January 2021
10.1126/sciadv.abe0726

Citation: M. Xing, Y. Jiang, W. Bi, L. Gao, Y.-L. Zhou, S.-L. Rao, L.-L. Ma, Z.-W. Zhang, H.-T. Yang, J. Chang, Strontium ions protect hearts against myocardial ischemia/reperfusion injury. *Sci. Adv.* **7**, eabe0726 (2021).